A Multi-Cluster-Based Distributed CDD Scheme for Asynchronous Joint Transmissions in Local and Private Wireless Networks

Kyeong Jin Kim, *Senior Member, IEEE*, Phee Lep Yeoh, *Member, IEEE*, Hongwu Liu, *Senior Member, IEEE*, Jianlin Guo, *Senior Member, IEEE*, Philip V. Orlik, *Senior Member, IEEE*, Yukimasa Nagai, *Senior Member, IEEE*, and H. Vincent Poor, *Life Fellow, IEEE*

***Abstract*— In this paper, a multiple cluster-based transmission diversity scheme is proposed for asynchronous joint transmissions (JT) in private networks. The use of multiple clusters or small cells is adopted to reduce the transmission distance to users thereby increasing data-rates and reducing latency. To further increase the spectral efficiency and achieve flexible spatial degrees of freedom, we consider that a distributed remote radio unit system (dRRUS) is installed in each of the clusters. A key characteristic of deploying the dRRUS in private networks is the associated multipath-rich and asynchronous delay propagation environment. Therefore, we consider asynchronous multiple signal reception at the remote radio units and propose an intersymbol interference free distributed cyclic delay diversity (dCDD) scheme for JT to achieve the full transmit diversity gain without requiring full channel state information of the private network. The spectral efficiency of the proposed dCDD-based JT is analyzed by deriving a new closed-form expression, and then compared with link-level simulations for non-identically distributed frequency selective fading over the entire network. Due to its distributed structure, the dRRUS relies on backhaul communications between the private network server and cluster master (CM), which is the main backhaul connection, and between the CM to remote radio units, which are the secondary backhaul connections. Thus, it is important for us to investigate the impact of reliability of main and secondary backhaul connections on the system. Our results show that the resulting composite backhaul connections can be accurately modeled by our proposed product of independent Bernoulli processes.**

***Index Terms*— Local and private 5G networks, distributed cyclic delay diversity, joint transmission, spectral efficiency.**

Manuscript received November 22, 2020; revised April 19, 2021; accepted June 18, 2021. Date of publication July 8, 2021; date of current version January 10, 2022. This work was supported in part by the U.S. National Science Foundation under Grant CCF-1908308, in part by the NSFC under Grant 6207010348, and in part by the NSF of Shandong Province under Grant ZR2020MF009. This article were presented in part at the 2020 IEEE Global Communications Conference, Taipei, Taiwan, December 2020 [1], and in part at the 2021 IEEE International Conference on Communications, Montreal, Canada, June 2021 [2]. The associate editor coordinating the review of this article and approving it for publication was X. Wang. *(Corresponding author: Kyeong Jin Kim.)*

Kyeong Jin Kim, Jianlin Guo, and Philip V. Orlik are with Mitsubishi Electric Research Laboratories (MERL), Cambridge, MA 02139 USA (e-mail: kkim,guo@merl.com; porlik@merl.com).

Phee Lep Yeoh is with the School of Electrical and Information Engineering, The University of Sydney, Sydney, NSW 2006, Australia (e-mail: phee.yeoh@sydney.edu.au).

Hongwu Liu is with the School of Information Science and Electrical Engineering, Shandong Jiaotong University, Jinan 250357, China (e-mail: hong.w.liu@hotmail.com).

Yukimasa Nagai is with Mitsubishi Electric Corporation, Kamakura, Kanagawa 2478501, Japan (e-mail: nagai.yukimasa@ds.mitsubishielectric.co.jp).

H. Vincent Poor is with the Department of Electrical and Computer Engineering, Princeton University, Princeton, NJ 08544 USA (e-mail: poor@princeton.edu).

Color versions of one or more figures in this article are available at https://doi.org/10.1109/TWC.2021.3093815.

Digital Object Identifier 10.1109/TWC.2021.3093815

I. Introduction

A LOCAL and private wireless network (LPWN) is a promising new in-building connectivity model offering previously unavailable wireless network performance to businesses and individuals. The owners of the LPWN can optimize services within their facility by planning and installing their own networks, and ensure reliable communications with exclusive use of all available radio and network resources. Private network can freely determine how resources are utilized, traffic is prioritized, or how a specific security standard is deployed. Potential applications for industries, businesses, utilities, and public sectors have gravitated towards 5G wireless networks with stringent performance requirements, in terms of availability, reliability, latency, device density, and throughput [3], which are also feasible in the shared spectrum or unlicensed spectrum used by the LPWN. Furthermore, to increase transmission speeds and capacity, reduce latency, and shorten the transmission distance to the users, a dense deployment of small cells or clusters is expected in LPWNs [4].

To increase the spectral efficiency and coverage, and to achieve flexible spatial degrees of freedom, a distributed antenna system (DAS), in which multiple antennas are installed over a single base station (BS) coverage area [5]–[13], is a promising approach for LPWNs. To exploit these benefits, the DAS has also been considered for indoor communication systems [12], [13] using multiple remote radio units (RRUs), each equipped with a single antenna and fixed power for signal processing due to a limited transmission power, which is known as a distributed remote radio unit system (dRRUS) [14]. Note that each RRU applies only a shifting operation to the input transmission symbol block. When each antenna operates as a BS, the DAS can be recognized as a coordinated multiple point (CoMP) system [15], [16]. The key advantage of CoMP is to support simultaneous

1536-1276 © 2021 IEEE. Personal use is permitted, but republication/redistribution requires IEEE permission.
See https://www.ieee.org/publications/rights/index.html for more information.

Authorized licensed use limited to: Princeton University. Downloaded on May 27,2022 at 01:57:22 UTC from IEEE Xplore. Restrictions apply.

communications by a plurality of BSs to a single or multiple users to improve the rate over a whole communication region. The two main forms of CoMP are coordinated beamforming and joint transmissions (JT). However, since we do not assume full channel state information at the transmitter (CSIT), we will focus on JT in this paper. Although geographically placed BSs should carefully consider path loss and shadowing [17], it is challenging to collect full CSIT at all the distributed transmitters. Furthermore, whilst reliable channel estimate can be obtained at the user, the feedback overhead will be huge as the number of BSs increases.

In addition, a tight clock synchronization among BSs is a critical challenge for simultaneous BS transmissions using JT CoMP [6], [9], [18]. This is because mismatch among BSs will cause interference at the user due to the difference in signal arrival time. However, for indoor LPWN environments such as in factories or office buildings, Global Navigation Satellite System signals are usually not available, so that an alternative clock synchronization method such as over the air synchronization could be implemented using wireless backhaul links [19].

With the proliferation of ultra-dense small cells, wireless backhauls should be carefully designed to support high speed data transportation from network nodes to end terminals and vice versa. Resulted by non-line-of-sight (nLoS) propagation, severe fading, and imperfect synchronization, backhaul unreliability inherent from wireless impairments is a key factor that affects wireless networks. In [20], mmWave communication technique was adopted in backhaul connections for 5G networks and the impact of nLoS propagation on backhaul reliability was investigated. For CoMP downlink cellular networks, the impacts of backhaul unreliability on the system performance were investigated in [21]. For distributed maximal ratio transmission (dMRT) [22], [23], the backhaul reliability was firstly modeled as a Bernoulli process. Since then, this model has been employed in various systems such as for physical layer security and spectrum sharing. To ensure successful implementations of JT in LPWNs, we aim to address the following three challenges.

1) CSIT-dependent precoders are usually employed to minimize interference caused by simultaneous multiple transmissions. To achieve this, full CSI feedback is necessary between the RX and DAS, which is challenging over the distributed system, and its overhead increases in proportion to the number of RRUs. Thus, it is necessary to develop an interference-free transmission scheme that requires only limited CSI.
2) When a DAS is deployed in LPWN environments, we will need to model the impact of multipath-rich propagation. Given that the distance between the RRUs varies with respect to the receiver (RX), interference will be an intrinsic challenge since the received symbol timing cannot be aligned at the RX due to path dependent propagation delay [24].
3) Hierarchical wireless backhaul communications are required in dRRUS, and thus it is necessary to investigate the impact of the backhaul reliability on the performance in private networks.

Taking into consideration of three challenging problems, we can summarize the following three advances compared with existing works [5]–[13].

1) A new multi-cluster-based distributed remote radio unit system (MC-dRRUS): To achieve high throughput in the private network, we propose a new MC-dRRUS, in which the private network server (PNS) provides transmission signals and synchronization to the respective cluster masters (CMs). Within non-overlapping clusters, each CM forms an individual dRRUS. It is desired to increase the number of RRUs to improve coverage over a large network area and to increase channel diversity. However, increasing the RRUs without clustering would result in increased interference, difficulty in time synchronization, and additional feedback overhead. In addition, due to the use of dCDD, the maximum number of RRUs that can be connected to the CM is limited. Thus, to deploy a large number of RRUs without increasing interference, simplifying synchronization among distributed RRUs, and maintaining a similar distribution of propagation delays, it is desirable to deploy multiple clusters of RRUs.
2) Distributed asynchronous cyclic delay diversity-based JT (dACDD-JT) scheme: Based on the distribution of propagation delays over all transmission paths, the CM is able to assign a variable CDD delay at each of its RRUs, which is necessary to remove intersymbol interference (ISI) caused by asynchronous signal reception at the RX [25]. Thus, by converting to synchronous signal reception, MC-dRRUS can bring benefits to LPWN industrial grade reliability.
3) Hierarchical wireless backhaul reliability model: By using a new Bernoulli process that is modeled by the product of independent Bernoulli processes, the impact of the main and secondary wireless backhaul reliability on the outage probability and spectral efficiency of the MC-dRRUS is investigated.

In summary, we propose a new system, MC-dRRUS in LPWN, utilizing dACDD-JT for different propagation delays over all transmission paths in multipath-rich environments. To draw insightful performance gain and limits, we conduct theoretical performance analysis for the outage probability and spectral efficiency.

A. Organization

The rest of the paper is organized as follows. In Section II, system and channel models are introduced. In Section III, dACDD-JT for cyclic prefixed single carrier (CP-SC) transmissions is introduced. The spectral efficiency and outage probability of the proposed dACDD-JT achieved by the MC-dRRUS is derived in Section IV. The outage probability and spectral efficiency of the dACDD-JT with unreliable backhaul connections is conducted in Section V. Simulation results are illustrated in Section VI and conclusions are drawn in Section VII.

Notation: $\mathbb{N}_0$ denotes the set of non-negative integers; $\mathbb{B}$ denotes the binary set composed of 0 and 1; $\mathbb{C}$ denotes

Authorized licensed use limited to: Princeton University. Downloaded on May 27,2022 at 01:57:22 UTC from IEEE Xplore. Restrictions apply.

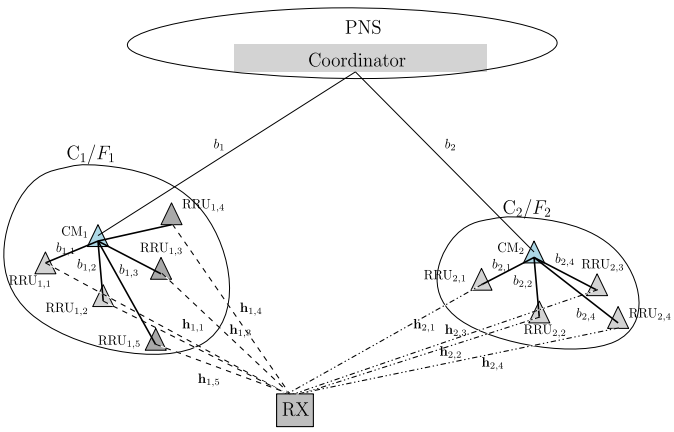

Fig. 1. Illustration of the proposed MC-dRRUS with five RRUs in Cluster 1, C_1, and four RRUs in Cluster 2, C_2. Two central nodes highlighted in each cluster are assigned as CMs to control the other RRUs in its cluster.

the set of complex numbers; $\boldsymbol{I}_N$ denotes an $N \times N$ identity matrix; $\mathbf{0}$ denotes an all-zero matrix of an appropriate size; $\mathcal{CN}\left(\mu, \sigma^2\right)$ denotes a complex Gaussian distribution with mean μ and variance σ^2; and $\mathbb{C}^{m\times n}$ denotes the vector space of all $m \times n$ complex matrices. $F_{\varphi}(\cdot)$ denotes the cumulative distribution function (CDF) of the random variable (RV) φ, whereas its probability density function (PDF) is denoted by $f_{\varphi}(\cdot)$. The binomial coefficient is denoted by $\binom{n}{k} \triangleq \frac{n!}{(n-k)!k!}$. For a vector $\boldsymbol{a}$, $\mathbb{L}(\boldsymbol{a})$ denotes the cardinality; its lth element is denoted by $\boldsymbol{a}(l)$; and the right circulant matrix determined by $\boldsymbol{a}$ is denoted by $\mathrm{RC}(\boldsymbol{a})$. For another vector $\boldsymbol{a}_{i,N}$ with the second subscript defining its cardinality, $\mathrm{sum}(\boldsymbol{a}_{i,N}) = c$ denotes the sum for all sets of positive indices of $\{\boldsymbol{a}_i(1), \ldots, \boldsymbol{a}_i(N)\}$ satisfying $\sum_{j=1}^{N} \boldsymbol{a}_i(j) = c$; the multinomial coefficient is defined as $\binom{c}{\boldsymbol{a}_{i,N}} \triangleq \frac{c!}{(\boldsymbol{a}_{i,N}(1))!(\boldsymbol{a}_{i,N}(2))!\ldots(\boldsymbol{a}_{i,N}(N))!}$; and $\sum^{a}_{\substack{n_1,\ldots,n_J \\ n_1\neq n_2\neq\ldots\neq n_J}} \triangleq \sum_{n_1=1}^{a} \sum_{\substack{n_2=1 \\ n_2\neq n_1}}^{a} \cdots \sum_{\substack{n_J=1 \\ n_J\neq n_1,\ldots,n_J\neq n_{J-1}}}^{a}$. For a set of continuous random variables, $\{x_1, x_2, \ldots, x_N\}$, $x_{\langle i \rangle}$ denotes the ith smallest random variable, which corresponds to the ith order statistic. For these order statistics, the spacing statistics, $\{y_1, \ldots, y_N\}$, are obtained by changing the variables as $y_i = x_{\langle i \rangle} - x_{\langle i-1 \rangle}$ with $y_1 = x_{\langle 1 \rangle}$.

II. System and Channel Models

Fig. 1 presents the proposed MC-dRRUS with two non-overlapping clusters, with each cluster considered as a dRRUS. When carrier aggregation is employed, C_2 can operate on a carrier, F_2, different from the carrier F_1 deployed in C_1. We consider that the PNS is the central grand master clock implemented using the precision time protocol (PTP) [26], [27], so that the CM[1] and RRUs can achieve clock synchronization with respect to the PNS. In contrast, the clocks at the CM and RRUs serve as the boundary clock and transparent clocks, respectively, which have multiple PTP ports to interact with other clocks. Moreover, we assume that the RX operates with an ordinary clock. We assume that wireless backhaul links, $\{b_1, b_2\}$, are configured to provide main backhaul access to the clusters from the coordinator at the PNS. Wireless backhaul links, denoted as $\{b_{i,j}, i = 1, 2, j = 1, \ldots, K\}$, provide secondary backhaul access from the CM to RRUs. We first assume ideal backhaul links in the following and consider non-ideal in Section IV. The CM is responsible for assigning the transmit signals for all RRUs. Every node in the cluster are assumed to have a single antenna. Since the RX receives signals from multiple clusters, it can adopt the single-user-multiple input and single output mode of operation to achieve a high throughput. In addition, due to the use of cooperative CP-SC transmissions, this system can effectively exploit the diversity in multipath-rich environments.

[1]The wireless access point in each dRRUS can serve as the CM using IEEE 802.11be. For multiple coexisting users, a cluster-based non-orthogonal multiple access (NOMA) scheme can be developed based on the dCDD-based cooperative pseudo-NOMA, which was recently proposed by [28].

A. Channel Model

A frequency selective fading channel from the kth RRU, deployed in the ith cluster, to the RX is denoted by $\boldsymbol{h}_{i,k}$ with $\mathbb{L}(\boldsymbol{h}_{i,k}) = N_{i,k}$. The distance-dependent large scaling fading is denoted by $\alpha_{i,k}$. For a distance $\vartheta_{i,k}$ from $\mathrm{RRU}_{i,k}$ to the RX, $\alpha_{i,k}$ is defined as $\alpha_{i,k} = (\vartheta_{i,k})^{-\epsilon}$, where ϵ denotes the path loss exponent. The RX is placed at a specific location with respect to the RRUs, and, thus, independent but non-identically distributed (i.n.i.d.) frequency selective fading channels from the RRUs to RX are considered in the dRRUS. The RX is assumed to know the number of multipath components in its receive channel using an initial training sequence [29] or adding a pilot as the suffix to each symbol block [30]. The RX first computes $N_{\max} \triangleq \max\{N_{i,k}, \forall i, k\}$, and then feeds back $N_{\max}$ to the PNS via one of the channels that results in the greatest channel strength and its corresponding secondary and main backhaul link, so that the CMs do not need to cooperate via the X2 interface to exchange relevant channel parameters. Except for the case of losing $N_{\max}$ or sudden changes in the channels while feeding back from the RX, there will be no performance loss. Thus, we assume that there is no loss of $N_{\max}$ and the channels are quasi-statistic during the feed back phase.

1) Diversity Analysis in Multipath-Rich Environments: As an illustrative example, we consider a system with one cluster and a single RRU. The cyclic-prefix (CP) length, N_{CP}, is set to $N_{1,1}$. When the CP-related signal part is removed at the RX, the received signal is given by

$$\boldsymbol{r} = \sqrt{P_T \alpha_{1,1}} \boldsymbol{H}_1 \boldsymbol{s} + \boldsymbol{z} \tag{1}$$

where P_T is the transmission power for single carrier transmissions, $\boldsymbol{s} \in \mathbb{C}^{Q\times 1}$ is the input transmission symbol block with the block size, Q, $\boldsymbol{z} \sim \mathcal{CN}(\mathbf{0}, \sigma_z^2 \boldsymbol{I}_Q)$, and $\boldsymbol{H}_1 = \mathrm{RC}([\boldsymbol{h}_{1,1}^T, \mathbf{0}_{1,Q-N_{1,1}}]^T)$. It has been verified by [31] that when a maximum likelihood detector (MLD) is applied, the signal-to-noise ratio (SNR) realized at the RX is given by $\gamma_1 = P_T \alpha_{1,1} \sum_{i=1}^{N_{1,1}} |\boldsymbol{h}_{1,1}(i)|^2 / \sigma_z^2$. According to this SNR, a multipath diversity of $N_{1,1}$ is achievable by CP-SC transmissions over the frequency selective fading channels [31].

Authorized licensed use limited to: Princeton University. Downloaded on May 27,2022 at 01:57:22 UTC from IEEE Xplore. Restrictions apply.

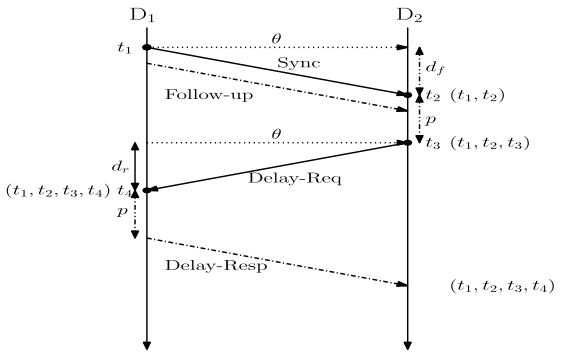

Fig. 2. Two-way packet exchange for synchronization. A filled circle dot denotes a timestamp in the event message recorded at its transmission and reception. The processing time taken at all the nodes is assumed to be p.

B. Two-Way Synchronization

To estimate the clock offset, θ, and propagation delay, d, the PTP as defined in [26], [27] specifies four event messages, known as Sync, Delay-Req, Pdelay-Req, and Pdelay-Resp, within which an accurate hardware timestamp is generated and recorded at transmission and reception of its respective messages. As shown in Fig. 2, after exchanging two-way packets between two PTP nodes D_1 and D_2, four hardware timestamps, (t_1, t_2, t_3, t_4), are available at D_1 and D_2. Based on these four timestamps and when clocks are perfectly synchronized in frequency and phase, d and θ are respectively computed as $d \approx ((t_4 + t_2) - (t_3 + t_1))/2$ and $\theta \approx ((t_3 - t_1) - (t_4 - t_2))/2$, where we have assumed that the forward propagation delay, d_f, is almost equal to the backward propagation delay, d_r, i.e., $d_f \approx d_r$. Applying the same procedure, D_1 can estimate the propagation delay to another PTP node, D_3, which is synchronized to D_2 [27]. Thus, when D_1 and D_2 are respectively recognized as the PNS and CM, then the PNS can have knowledge of the propagation delays for all RRUs connected to this CM. When multiple RXs or users co-exist in the network, multiple domains are formed. Each domain is composed of a multi-level hierarchical PTP and a particular RX or user. Since boundary and transparent clocks can have multiple PTP ports, each domain has its own synchronization process without being affected by other domains. Thus, the employed synchronization procedure can be extended to the case with multiple RXs or users. Due to the existing frequency drift and phase offset between the clocks at D_1 and D_2, the clock synchronization should be continuously adjusted to set their values to approximately zero. Note that two-way synchronization is accomplished via the main and secondary backhaul connections.

Referring to Figs. 1 and 2, the PNS has a set of propagation delay estimates $\{d_{1,k}\}_{k=1,\ldots,K}$ over the cluster C_1. For the cluster C_2, the PNS can also estimate another set of propagation delays. Thus, we can assume that a complete set of propagation delays, $\{d_{i,k}\}_{i=1,2 \text{ and } k=1,\ldots,K}$, is available at the PNS by employing PTP. According to this set, the PNS computes the propagation delay for the signal that arrives first at the RX as $d_{\mathrm{ref}} \triangleq \min(\{d_{i,k}\}_{i=1,2 \text{ and } k=1,\ldots,K})$. Then, the relative propagation delay with respect to d_{ref} can be expressed as:

$$\delta d_{i,k} \triangleq d_{i,k} - d_{\mathrm{ref}}, \quad \text{for } i = 1, 2 \text{ and } k = 1, \ldots, K. \quad (2)$$

The multi-level hierarchical PTP allows the PNS to break the dependency of different dRRUS clusters to the common PNS, and thus each cluster can adopt dACDD independently from another cluster.

C. Summary of Distributed CDD

The dCDD scheme was proposed by [14] for distributed CP-SC transmissions to achieve transmit diversity without requiring full CSIT. Depending on the block size, Q, of the transmission symbol, $\boldsymbol{s} \in \mathbb{C}^{Q \times 1}$, and the cyclic-prefix (CP) length, N_{CP}, which is set to $N_{\max}$, the maximum number of RRUs that can support ISI-free reception at the RX, is determined by $M = \lfloor Q/N_{\mathrm{CP}} \rfloor$, where $\lfloor \cdot \rfloor$ denotes the floor function.

1) Overpopulated dRRUS: When the ith dRRUS is overpopulated with RRUs, i.e., $K_i > M$, the CM_i needs to select only M RRUs for dCDD operation. Thus, the RX needs to feed back the relevant channel information to the CM_i via the PNS. Based on available channel estimates, the RX arranges all the RRUs from smallest to largest, as follows:

$$\alpha_{i,\langle 1 \rangle} \|\boldsymbol{h}_{i,\langle 1 \rangle}\|^2 \leq \ldots \leq \alpha_{i,\langle K_i \rangle} \|\boldsymbol{h}_{i,\langle K_i \rangle}\|^2. \quad (3)$$

According to (3), the RX forms a list specifying the strength order, that is, $\mathbb{D}_i \triangleq (\langle 1 \rangle, \ldots, \langle K_i \rangle)$, and then feeds back $\mathbb{D}_i$ to the PNS. Using backhaul communications over the main backhaul b_i, CM_i can have $\mathbb{D}_i$, from which CM_i selects the M RRUs indexed by the last M elements of $\mathbb{D}_i$, that is, $\mathrm{RRU}_{i,\langle K_i - M + 1 \rangle}, \ldots, \mathrm{RRU}_{i,\langle K_i \rangle}$. The remaining $K_i - M$ RRUs are controlled by CM_i to be idle from communications. For the chosen M RRUs, CM_i assigns the CDD delay to $\mathrm{RRU}_{i,\langle K_i - M + m \rangle}$ as follows:

$$\Delta_m = (m-1) N_{\mathrm{CP}}, \ m = 1, \ldots, M. \quad (4)$$

2) Underpopulated and Full-Populated dRRUSs: When the ith dRRUS is either underpopulated or full-populated with RRUs, i.e., $K_i \leq M$, the CM_i uses all K_i RRUs for dCDD operation. Thus, the RX does not need to feed back a list of the channel strength order, $\mathbb{D}_i$. Similar to the overpopulated dRRUS, CM_i assigns the CDD delay to $\mathrm{RRU}_{i,k}$ as follows:

$$\Delta_k = (k-1) N_{\mathrm{CP}}, \quad k = 1, \ldots, K_i. \quad (5)$$

Due to the simple linear relationship in both (4) and (5), we consider the linear CDD assignment.[2] Note that, for overpopulated, underpopulated, and full-populated dRRUSs, the PNS can achieve the same diversity gain as that of dMRT [22], [23] using only partial CSIT. In particular, [23] verified the achievable diversity gain over non-identical Nakagami-m fading channel. Since the overpopulated dRRUS is more realistic in practical problems, we will mainly consider it in this paper. In summary, for dCDD operation, the PNS needs to know M, N_{CP}, and $\mathbb{D}_i$, which are available at each of the CMs by main backhaul communications from the PNS.

[2]In contrast to the linear CDD assignment, a random CDD assignment was proposed by [32]. However, the performance is irrespective of the CDD assignment only if one CDD delay is exclusively assigned to one RRU [14].

Authorized licensed use limited to: Princeton University. Downloaded on May 27,2022 at 01:57:22 UTC from IEEE Xplore. Restrictions apply.

III. DACDD-JT for CP-SC Transmissions

In this section, we first describe the received signal at the RX taking account variations in the propagation delays. Without loss of generality, we assume that $\mathrm{RRU}_{i,1}$'s signal arrives first. Since the PNS has propagation delay estimates for all the nodes, it can compute the distribution of all other relative propagation delays with respect to the propagation delay of the $\mathrm{RRU}_{i,1}$'s signal. As an initial interactive process between the PNS and RX, the PNS transmits d_{ref} to the RX via the main and secondary backhaul links in each cluster.

After the removal of the CP signal and applying post-processing by $d_{1,1}$, the RX receives a composite signal from two clusters, which respectively have K_1 and K_2 RRUs, given by (6) provided at the bottom of the next page. In (6), $[\cdot]_{J_1}$ and $[\cdot]_{J_2}$ respectively represent the composite signals transmitted from C_1 and C_2. In (6), P_T is the transmission power for single carrier transmissions, and $\boldsymbol{H}_{i,\langle K_i-M+m\rangle} \in \mathbb{C}^{Q\times Q}$ is a right circulant matrix determined by $\boldsymbol{h}_{i,\langle K_i-M+m\rangle}$. In addition, $\boldsymbol{\Pi}_{i,\langle K_i-M+m\rangle} \in \mathbb{B}^{Q\times Q}$ is a right circulant and orthogonal permutation matrix determined by $\delta d_{i,\langle K_i-M+m\rangle} \in \mathbb{N}_0$. Since full CSIT is not available in the considered system, the same P_T is assigned to all the RRUs. By shifting down $\boldsymbol{I}_Q$ by $\delta d_{i,\langle K_i-M+m\rangle}$ rows, $\boldsymbol{\Pi}_{i,\langle K_i-M+m\rangle}$ can be obtained. An additional set of permutation matrices, $\{\boldsymbol{P}_{i,\langle K_i-M+m\rangle}, \forall i, m\}$, will be defined later. The additive vector noise is denoted by $\boldsymbol{z} \sim \mathcal{CN}(\boldsymbol{0}, \sigma_z^2\boldsymbol{I}_Q)$. For proper operation, we assume that $0 \le d_{i,\langle K_i-M+m\rangle} \le N_{\mathrm{CP}}$, so that the relative propagations are also given by $0 \le \delta d_{i,\langle K_i-M+m\rangle} \le N_{\mathrm{CP}}$ [24], [25].

A. DACDD for JT

Using the properties of the right circulant matrix, (6) can be rewritten as follows:

$$\boldsymbol{r} = \sum\nolimits_{m=1}^{M} \sqrt{P_T\alpha_{1,\hat{m}_1}}\boldsymbol{H}_{1,\hat{m}_1}\boldsymbol{\Pi}_{1,\hat{m}_1}[\boldsymbol{P}_{1,\hat{m}}\boldsymbol{s}]_{J_3} + \sum\nolimits_{m=1}^{M} \sqrt{P_T\alpha_{2,\hat{m}_2}}\boldsymbol{H}_{2,\hat{m}_2}\boldsymbol{\Pi}_{2,\hat{m}_2}[\boldsymbol{P}_{2,\hat{m}_2}\boldsymbol{s}]_{J_4} + \boldsymbol{z} \quad (7)$$

where $\hat{m}_i \triangleq \langle K_i - M + m\rangle$. Furthermore, $[\cdot]_{J_3}$ and $[\cdot]_{J_4}$ correspond to local operations respectively performed at $\mathrm{RRU}_{1,\hat{m}_1}$ and $\mathrm{RRU}_{2,\hat{m}_2}$. To achieve ISI-free reception at the RX, it is required that $\boldsymbol{\Pi}_{1,\hat{m}_1}\boldsymbol{P}_{1,\hat{m}_1}$ and $\boldsymbol{\Pi}_{2,\hat{m}_2}\boldsymbol{P}_{2,\hat{m}_2}$ are orthogonal and right circulant matrices [25], and meet either the random CDD delay assignment or linear CDD delay assignment for $\mathrm{RRU}_{i,\hat{m}_i}$. Accordingly, we can readily obtain $\delta T_{i,\hat{m}_i} \in \mathbb{N}_0$ that meets the condition: $\Delta_{\hat{m}_i} = \delta d_{i,\hat{m}_i} + \delta T_{i,\hat{m}_i}$. Thus, for operation $[\cdot]_{J_3}$, $\mathrm{RRU}_{1,\hat{m}_1}$ assigns $\delta T_{1,\hat{m}_1}$ as its CDD delay rather than $\Delta_{\hat{m}_1}$. By circularly shifting down the transmission symbol $\boldsymbol{s}$ by $\delta T_{1,\hat{m}_1}$, $[\cdot]_{J_3}$ can be accomplished. Similar operation is conducted for $[\cdot]_{J_4}$. Thus, $\boldsymbol{P}_{1,\hat{m}_1}$ and $\boldsymbol{P}_{2,\hat{m}_2}$ can be obtained from $\boldsymbol{I}_Q$ by circularly shifting down respectively by $\delta T_{1,\hat{m}_1}$ and $\delta T_{2,\hat{m}_2}$.

The ISI caused by variable propagation delays and multiple single carrier transmissions can be removed by a series of circular shifting operations that are respectively performed by the RRUs, and caused by channel propagation. Thus, we propose dACDD as a more general version of dCDD allowing a distribution of different propagation delays over the LPWN. For practical dACDD operation, the PNS needs to know all the $\{d_{i,\hat{m}_i}\}_{i=1,2 \text{ and } m=1,\ldots,M}$ and $\{\delta d_{i,\hat{m}_i}\}_{i=1,2 \text{ and } m=1,\ldots,M}$. We assume that this can be achieved using PTP, where the delays are computed without additional feedback from the RX, which is the key difference of this paper compared to [25], which did not consider PTP in LPWNs. Furthermore, in contrast to the general multiple transmissions, multiple CP-SC transmissions do not cause any ISI when dACDD is integrated with JT. Thus, it is not necessary to use multiple orthogonal channels to avoid ISI. This is one of the unique benefits of dACDD over [14]. To explain ISI-free processing, we provide the following example.

1) Example 1: Let us assume that $Q = 8$, $N_{1,1} = 2$, $N_{1,2} = 3$, $d_{1,1} = 1$, $d_{1,2} = 3$, $N_{2,1} = 4$, $N_{2,2} = 3$, $d_{2,1} = 2$, $d_{2,2} = 4$. Then, we can have $N_{\mathrm{CP}} = 4$, $\delta d_{1,1} = 0$, $\delta d_{1,2} = 2$, $\delta d_{2,1} = 1$, and $\delta d_{2,2} = 3$, so that $\delta T_{1,1} = 0$, $\delta T_{1,2} = 2$, $\delta T_{2,1} = 7$, $\delta T_{2,2} = 1$. Based on these computations, $\boldsymbol{H}_{1,\mathrm{eq}} \triangleq \sum_{m=1}^{2}\boldsymbol{H}_{1,m}\boldsymbol{\Pi}_{1,m}\boldsymbol{P}_{1,m}$ and $\boldsymbol{H}_{2,\mathrm{eq}} \triangleq \sum_{m=1}^{2}\boldsymbol{H}_{2,m}\boldsymbol{\Pi}_{2,m}\boldsymbol{P}_{2,m}$ are respectively given by (8) shown at the bottom of the next page. Recall that $\boldsymbol{h}_{i,m}(l)$ denotes the lth element of $\boldsymbol{h}_{i,m}$. Again from the properties of the right circulant matrix, $\boldsymbol{H}_{1,\mathrm{eq}}$ and $\boldsymbol{H}_{2,\mathrm{eq}}$ are respectively determined by the first column vectors, that is, $\boldsymbol{H}_{1,\mathrm{eq}} = \mathrm{RC}([\boldsymbol{h}_{1,1}^T, \boldsymbol{0}_{1\times 2}^T, \boldsymbol{h}_{1,2}^T, \boldsymbol{0}_{1\times 1}]^T)$ and $\boldsymbol{H}_{2,\mathrm{eq}} = \mathrm{RC}([\boldsymbol{h}_{2,2}^T, \boldsymbol{h}_{2,1}^T, \boldsymbol{0}_{1\times 1}]^T)$. From (8), we can see that channel elements do not overlap with each other in the equivalent channel matrices, so that dACDD achieves ISI-free CP-SC transmissions from a plurality of clusters. That is, each cluster is independent of transmissions from other clusters. It has been verified that performance of the system with CP-SC transmissions is mainly determined by the magnitude of the first column vector of the equivalent channel matrix [31]. Thus, another system whose equivalent channel matrix, represented by $\boldsymbol{H}_{3,\mathrm{eq}} = \mathrm{RC}([\boldsymbol{h}_{2,1}^T, \boldsymbol{0}_{1\times 1}, \boldsymbol{h}_{2,2}^T,]^T)$, will have the same performance as the system with $\boldsymbol{H}_{2,\mathrm{eq}}$. From Example 1, $\boldsymbol{H}_{3,\mathrm{eq}}$ can be obtained by applying different CDD delays such as $\delta T_{2,1} = 3$ and $\delta T_{2,2} = 5$.

IV. Spectral Efficiency and Outage Probability of DACDD-JT in Multi-Cluster Systems

Using the properties of the right circulant matrix, the achievable SNR realized by dACDD-JT in multi-cluster systems can be derived by the following *Theorem 1*.

Theorem 1: Based on the proposed multi-cluster-dACDD (MC-dACDD) scheme in Section III, ISI-free reception can be achieved at the RX. Thus, the achievable SNR realized by JT is given by

$$\gamma_{\mathrm{JT}} = \rho\big(\sum\nolimits_{m=1}^{M}\alpha_{1,\hat{m}_1}\|\boldsymbol{h}_{1,\hat{m}_1}\|^2 + \sum\nolimits_{m=1}^{M}\alpha_{2,\hat{m}_2}\|\boldsymbol{h}_{2,\hat{m}_2}\|^2\big) = \gamma_{\mathrm{JT},1} + \gamma_{\mathrm{JT},2} = \rho_s/\sigma_z^2 \quad (9)$$

where $\rho_s = P_T\big(\sum_{m=1}^{M}\alpha_{1,\hat{m}_1}\|\boldsymbol{h}_{1,\hat{m}_1}\|^2 + \sum_{m=1}^{M}\alpha_{2,\hat{m}_2}\|\boldsymbol{h}_{2,\hat{m}_2}\|^2\big)$ and $\gamma_{\mathrm{JT},i} \triangleq \rho\sum_{m=1}^{M}\alpha_{i,\hat{m}_i}\|\boldsymbol{h}_{i,\hat{m}_i}\|^2$ with $\rho \triangleq P_T/\sigma_z^2$.

Proof: When $\{\boldsymbol{h}_{1,\hat{m}_1}\}$ and $\{\boldsymbol{h}_{2,\hat{m}_2}\}$ are independent of each other, and $\boldsymbol{H}_{1,\mathrm{eq}}$ and $\boldsymbol{H}_{2,\mathrm{eq}}$ are right circulant, ρ_s,

Authorized licensed use limited to: Princeton University. Downloaded on May 27,2022 at 01:57:22 UTC from IEEE Xplore. Restrictions apply.

realized at the RX, is determined by the summation of their squared Euclidean norms. This signal power can be achievable when a MLD is applied at the RX [31]. With the use of MLD, the matrix multiplication made by two permutation matrices, $\boldsymbol{\Pi}_{i,\hat{m}_i}$ and $\boldsymbol{P}_{i,\hat{m}_i}$, has no distinctive impact on the achievable SNR. ■

For overpopulated dRRUS, the CM selects only M RRUs by referring to the channel strength. Thus, the order statistics are employed in the expression for the SNR. Based on *Theorem 1*, we can derive the following corollaries.

Corollary 1: Theorem 1 proves that by compensating different signal arrival times at the RX, the MC-dRRUS allows JT to achieve the same performance gains as dMRT without full CSIT at the PNS and CMs.

Furthermore, the following *Corollary* supports the use of dACDD-JT over the MC-dRRUS with carrier aggregation [33], [34].

Corollary 2: When the block size of $\boldsymbol{s}$ is the same, by combining two or more orthogonal carrier channels[3] as an aggregated channel, a higher spectral efficiency can be achieved due to the efficient use of fragmented spectrum.

Proof: By using a set of one or more non-overlapping frequency bands, an additional ISI-free JT can be achieved in the MC-dRRUS. Thus, a greater SNR can be realized at the RX, which directly increases the spectral efficiency. ■

Theorem 2: Applying the dACDD-JT scheme, the proposed MC-dRRUS results in a received SNR, γ_{JT}, whose moment geometric function (MGF) is given by

$$M_{\gamma_{\mathrm{JT}}}(s) = \widehat{\sum_{\substack{n_1,\ldots,n_M \\ n_1\neq\ldots\neq n_M}}} \widetilde{\sum_{\substack{\tilde{n}_1,\ldots,\tilde{n}_M \\ \tilde{n}_1\neq\ldots\neq\tilde{n}_M}}} \prod_{k=1}^{M}(M+1-k)^{-e_k} \times \Gamma(e_k)\prod_{k=1}^{M}(M+1-k)^{-\tilde{e}_k}\Gamma(\tilde{e}_k) \times \big[\prod_{k=1}^{2M}(s+Q_k)^{-E_k}\big]_{J_5} \tag{10}$$

where $Q_k = [q_1,\ldots,q_M,\tilde{q}_1,\ldots,\tilde{q}_M]$, and $E_k = [e_1,\ldots,e_M,\tilde{e}_1,\ldots,\tilde{e}_M]$. Additional terms are defined in Appendix A.

Proof: See Appendix A. ■

In general, as either M or $N_{\max}$ increases, the inverse MGF (IMGF) based on the partial fraction (PF) could easily diverge, thus it is necessary to develop a more reliable approximate expression for $[\cdot]_{J_5}$.

Corollary 3: A reliable and approximate expression for $[\cdot]_{J_5}$ is given by

$$\prod_{k=1}^{2M}(s+Q_k)^{-E_k} = \sum_{l=0}^{N_1}\delta_l(b_I)^{-l}(1/b_I+s)^{-G_d-l} \tag{11}$$

where $G_d \triangleq \sum_{k=1}^{2M}E_k$, $b_I \triangleq \min(1/Q_1,\ldots,1/Q_{2M})$, and $\delta_l \triangleq \frac{1}{l}\sum_{i=1}^{l} i r_i \delta_{l-i}$ with $\delta_0 = 1$ and $r_i = \sum_{j=1}^{2M}E_j(1-b_IQ_i)^j$. In addition, N_1 denotes the upper limit summation, which determines the accuracy of the approximation.

Proof: The approximation is based on the weighted summation derived in [35]. ■

Corollary 3 provides the MGF expressed by the weighted sum of N_1+1 terms, each of which is proportional to $(1/b_I+s)^{-G_d-l}$. Thus, the following corollary can be immediately derived.

Corollary 4: The CDF of γ_{JT} can be expressed by a finite number of gamma distributions. Its expression is given by (12) provided at the bottom of the next page. In (12), $\Gamma(\cdot)$ and $\Gamma_U(\cdot,\cdot)$ respectively denote complete gamma and incomplete upper-gamma functions.

It is worthwhile to note that b_I, G_d, and N_1 are key parameters in specifying the distributions of γ_{JT}. In particular, N_1 determines the approximation accuracy of the distributions represented by a finite number of gamma distributions. Theorem 2 provides the MGF for two clusters. Thus, for a general number of N_D clusters, the MGF for γ_{JT} is

[3]Note that three types of realization, that is, continuous intra-band, non-continuous intra-band, and non-continuous inter-band, can be possible.

$$\begin{aligned}\boldsymbol{r} = &\big[\sum_{m=1}^{M}\sqrt{P_T\alpha_{1,\langle K_1-M+m\rangle}}\boldsymbol{\Pi}_{1,\langle K_1-M+m\rangle}\boldsymbol{H}_{1,\langle K_1-M+m\rangle}\boldsymbol{P}_{1,\langle K_1-M+m\rangle}\boldsymbol{s}\big]_{J_1}\\ &+\big[\sum_{m=1}^{M}\sqrt{P_T\alpha_{2,\langle K_2-M+m\rangle}}\boldsymbol{\Pi}_{2,\langle K_2-M+m\rangle}\boldsymbol{H}_{2,\langle K_2-M+m\rangle}\boldsymbol{P}_{2,\langle K_2-M+m\rangle}\boldsymbol{s}\big]_{J_2}+\boldsymbol{z}\end{aligned} \tag{6}$$

$$\boldsymbol{H}_{1,\mathrm{eq}} = \begin{bmatrix} \boldsymbol{h}_{1,1}(1) & 0 & \boldsymbol{h}_{1,2}(3) & \boldsymbol{h}_{1,2}(2) & \boldsymbol{h}_{1,2}(1) & 0 & 0 & \boldsymbol{h}_{1,1}(2)\\ \boldsymbol{h}_{1,1}(2) & \boldsymbol{h}_{1,1}(1) & 0 & \boldsymbol{h}_{1,2}(3) & \boldsymbol{h}_{1,2}(2) & \boldsymbol{h}_{1,2}(1) & 0 & 0\\ 0 & \boldsymbol{h}_{1,1}(2) & \boldsymbol{h}_{1,1}(1) & 0 & \boldsymbol{h}_{1,2}(3) & \boldsymbol{h}_{1,2}(2) & \boldsymbol{h}_{1,2}(1) & 0\\ 0 & 0 & \boldsymbol{h}_{1,1}(2) & \boldsymbol{h}_{1,1}(1) & 0 & \boldsymbol{h}_{1,2}(3) & \boldsymbol{h}_{1,2}(2) & \boldsymbol{h}_{1,2}(1)\\ \boldsymbol{h}_{1,2}(1) & 0 & 0 & \boldsymbol{h}_{1,1}(2) & \boldsymbol{h}_{1,1}(1) & 0 & \boldsymbol{h}_{1,2}(3) & \boldsymbol{h}_{1,2}(2)\\ \boldsymbol{h}_{1,2}(2) & \boldsymbol{h}_{1,2}(1) & 0 & 0 & \boldsymbol{h}_{1,1}(2) & \boldsymbol{h}_{1,1}(1) & 0 & \boldsymbol{h}_{1,2}(3)\\ \boldsymbol{h}_{1,2}(3) & \boldsymbol{h}_{1,2}(2) & \boldsymbol{h}_{1,2}(1) & 0 & 0 & \boldsymbol{h}_{1,1}(2) & \boldsymbol{h}_{1,1}(1) & 0\\ 0 & \boldsymbol{h}_{1,2}(3) & \boldsymbol{h}_{1,2}(2) & \boldsymbol{h}_{1,2}(1) & 0 & 0 & \boldsymbol{h}_{1,1}(2) & \boldsymbol{h}_{1,1}(1) \end{bmatrix} \text{ and}$$

$$\boldsymbol{H}_{2,\mathrm{eq}} = \begin{bmatrix} \boldsymbol{h}_{2,2}(1) & 0 & \boldsymbol{h}_{2,1}(3) & \boldsymbol{h}_{2,1}(2) & \boldsymbol{h}_{2,1}(1) & \boldsymbol{h}_{2,2}(4) & \boldsymbol{h}_{2,2}(3) & \boldsymbol{h}_{2,2}(2)\\ \boldsymbol{h}_{2,2}(2) & \boldsymbol{h}_{2,2}(1) & 0 & \boldsymbol{h}_{2,1}(3) & \boldsymbol{h}_{2,1}(2) & \boldsymbol{h}_{2,1}(1) & \boldsymbol{h}_{2,2}(4) & \boldsymbol{h}_{2,2}(3)\\ \boldsymbol{h}_{2,2}(3) & \boldsymbol{h}_{2,2}(2) & \boldsymbol{h}_{2,2}(1) & 0 & \boldsymbol{h}_{2,1}(3) & \boldsymbol{h}_{2,1}(2) & \boldsymbol{h}_{2,1}(1) & \boldsymbol{h}_{2,2}(4)\\ \boldsymbol{h}_{2,2}(4) & \boldsymbol{h}_{2,2}(3) & \boldsymbol{h}_{2,2}(2) & \boldsymbol{h}_{2,2}(1) & 0 & \boldsymbol{h}_{2,1}(3) & \boldsymbol{h}_{2,1}(2) & \boldsymbol{h}_{2,1}(1)\\ \boldsymbol{h}_{2,1}(1) & \boldsymbol{h}_{2,2}(4) & \boldsymbol{h}_{2,2}(3) & \boldsymbol{h}_{2,2}(2) & \boldsymbol{h}_{2,2}(1) & 0 & \boldsymbol{h}_{2,1}(3) & \boldsymbol{h}_{2,1}(2)\\ \boldsymbol{h}_{2,1}(2) & \boldsymbol{h}_{2,1}(1) & \boldsymbol{h}_{2,2}(4) & \boldsymbol{h}_{2,2}(3) & \boldsymbol{h}_{2,2}(2) & \boldsymbol{h}_{2,2}(1) & 0 & \boldsymbol{h}_{2,1}(3)\\ \boldsymbol{h}_{2,1}(3) & \boldsymbol{h}_{2,1}(2) & \boldsymbol{h}_{2,1}(1) & \boldsymbol{h}_{2,2}(4) & \boldsymbol{h}_{2,2}(3) & \boldsymbol{h}_{2,2}(2) & \boldsymbol{h}_{2,2}(1) & 0\\ 0 & \boldsymbol{h}_{2,1}(3) & \boldsymbol{h}_{2,1}(2) & \boldsymbol{h}_{2,1}(1) & \boldsymbol{h}_{2,2}(4) & \boldsymbol{h}_{2,2}(3) & \boldsymbol{h}_{2,2}(2) & \boldsymbol{h}_{2,2}(1) \end{bmatrix} \tag{8}$$

Authorized licensed use limited to: Princeton University. Downloaded on May 27,2022 at 01:57:22 UTC from IEEE Xplore. Restrictions apply.

proportional to the following expression

$$\prod_{k=1}^{N_D M}(s+Q_k)^{-E_k}=\sum_{l=0}^{N_2}\delta_l(b_I)^{-l}(1/b_I+s)^{-G_d-l} \tag{13}$$

where $G_d \triangleq \sum_{k=1}^{N_D M} E_k$, $b_I \triangleq \min(1/Q_1,\ldots,1/Q_{N_D M})$, and $\delta_l \triangleq \frac{1}{l}\sum_{i=1}^{l} i r_i \delta_{l-i}$ with $\delta_0 = 1$ and $r_i = \sum_{j=1}^{N_D M} E_j(1-b_I Q_i)^j$. Similar to Q_k and E_k for two clusters, the corresponding terms can be derived for N_D clusters. To achieve the same level of an approximation accuracy, it is required that $N_2 \approx N_D N_1$. Thus, according to (13), the distributions of $\gamma_{\rm JT}$ realized by more than two clusters can be readily derived.

A. Spectral Efficiency

Based on (9), the spectral efficiency (SE) of JT realized by dACDD in multi-cluster systems is given by

$$\mathrm{SE}=\frac{1}{\log(2)}\int_0^\infty \frac{1-F_{\gamma_{\rm JT}}(x)}{1+x}dx. \tag{14}$$

Now using distributions of $\gamma_{\rm JT}$ provided by Corollary 4, the spectral efficiency is derived in the following theorem.

Theorem 3: The achievable spectral efficiency of the proposed dACDD based JT realized by MC-dRRUS is given by (15) provided at the bottom of the next page. In (15), $G_{p,q}^{m,n}\big(t\big|\begin{smallmatrix} a_1,\ldots,a_n,a_{n+1},\ldots,a_p \\ b_1,\ldots,b_m,b_{m+1},\ldots,b_q\end{smallmatrix}\big)$ denotes the Meijer G-function [36, Eq. (9.301)].

Proof: We first express the functions of x in terms of Meijer G-functions, i.e., $(1+x)^{-1}=G_{1,1}^{1,1}(x\big|\begin{smallmatrix}0\\0\end{smallmatrix})$ and $\Gamma_u(j,\alpha x)=G_{1,2}^{2,0}(\alpha x\big|\begin{smallmatrix}1\\j,0\end{smallmatrix})$. Next, applying [37, eq. (2.24.1,2)], we can derive (15). ∎

B. Outage Probability

Based on our closed-form expression for the CDF in (12), the outage probability can be readily obtained. At an outage SNR, $o_{\rm th}$, the outage probability is given by

$$\mathrm{OP}=F_{\gamma_{\rm JT}}(o_{\rm th}). \tag{16}$$

Theorem 4: When the dRRUS is overpopulated, the dACDD-JT achieves the asymptotic diversity gain in the high SNR region as follows:

$$G_d=\sum_{j=1}^{K_1}N_{1,j}+\sum_{j=1}^{K_2}N_{2,j}. \tag{17}$$

The same asymptotic diversity gain can be achieved for underpopulated MC-dRRUS.

Proof: See [31] for the diversity gain derivation of underpopulated dRRUS, whereas see Appendix B for the overpopulated dRRUS. ∎

Theorem 4 shows that a higher number of non-overlapped clusters results in a greater diversity gain for JT in proportion to the number of clusters when the dRRUS clusters do not cause inter-cluster and intra-cluster ISI at the receiver. In addition, as the dRRUS is more populated, a greater diversity gain is achieved. This is a more general result compared to [14], which verified the diversity gain only for identical fading channels and clock synchronized RRUs.

V. Outage Probability With Unreliable Backhaul Connections

In this section, we assume the practical scenario where the wireless backhaul connections may be unreliable and suffer from outages. Based on (7), the composite signal received at the RX from two clusters can be expressed as

$$\begin{aligned}\boldsymbol{r}=&\sum_{k=1}^{K_1}\sqrt{P_T\alpha_{1,k}}\mathbb{I}_{1,k}\boldsymbol{\Pi}_{1,k}\boldsymbol{H}_{1,k}[\boldsymbol{P}_{1,k}\boldsymbol{s}]_{L_1}\\&+\sum_{k=1}^{K_2}\sqrt{P_T\alpha_{2,k}}\mathbb{I}_{2,k}\boldsymbol{\Pi}_{2,k}\boldsymbol{H}_{2,k}[\boldsymbol{P}_{2,k}\boldsymbol{s}]_{L_2}+\boldsymbol{z}\end{aligned} \tag{18}$$

where $\mathbb{I}_{j,k}$ models the reliability of the kth secondary backhaul, $b_{j,k}$, within cluster C_j, via the jth main backhaul, b_j. It is assumed that two clusters are respectively populated by K_1 and K_2 RRUs with $K_1 \le M$ and $K_2 \le M$. When the backhaul reliability is modeled by a Bernoulli process [23], that is, $Pr(b_j=1)=p_j$, $Pr(b_j=0)=1-p_j$ and $Pr(b_{j,k}=1)=p_{j,k}$, $Pr(b_{j,k}=0)=1-p_{j,k}$, then we can specify a Bernoulli process $\mathbb{I}_{j,k}$ with $Pr(\mathbb{I}_{j,k}=1)=p_j p_{j,k} \triangleq R_{j,k}$ and $Pr(\mathbb{I}_{j,k}=0)=1-R_{j,k}$. In addition, $\boldsymbol{\Pi}_{j,k}$ is the permutation matrix specified by the relative propagation delay $\delta d_{j,k}$, which is similarly determined as that of the over-populated dRRUS. $\boldsymbol{H}_{i,k}$ is the right circulant matrix determined by $\boldsymbol{h}_{i,k}$. To achieve ISI-free reception at the RX, the permutation matrix, $\boldsymbol{P}_{j,k}$, needs to take into account $\delta d_{j,k}$ to meet (5), in such a way that $\Delta_k=\delta d_{j,k}+\delta T_{j,k}$. Then, $\boldsymbol{P}_{j,k}$ is determined from $\boldsymbol{I}_Q$ by circularly shifting down by $\delta T_{j,k} \in \mathbb{N}_0$. Thus, L_1 and L_2 correspond to local operations respectively performed at $\mathrm{RRU}_{1,k}$ and $\mathrm{RRU}_{2,k}$. Based on this proposed local processing, ISI caused by multipath fading and non-identical propagation delays can be mitigated and absorbed by dACDD.

Again using the properties of the right circulant matrix, the achievable SNR realized by dACDD-JT in multi-cluster systems and the corresponding MGF are respectively derived by the following *Theorem 5* and *Theorem 6*. Note that both Theorems jointly take into account unreliable main and secondary backhaul connections in the LPWN.

Theorem 5: Assuming unreliable main and secondary backhaul connections, the under-populated MC-dRRUS can still achieve ISI-free reception at the RX. Thus, the achievable SNR

$$\begin{aligned}F_{\gamma_{\rm JT}}(x)=1-&\widehat{\sum_{\substack{n_1,\ldots,n_M\\ n_1\neq\ldots\neq n_M}}}\ \widetilde{\sum_{\substack{\tilde{n}_1,\ldots,\tilde{n}_M\\ \tilde{n}_1\neq\ldots\neq\tilde{n}_M}}}\ \prod_{k=1}^{M}(M+1-k)^{-e_k}\Gamma(e_k)\\&\times\prod_{k=1}^{M}(M+1-k)^{-\tilde{e}_k}\Gamma(\tilde{e}_k)\sum_{l=0}^{N_1}\delta_l(b_I)^{-l}(b_I)^{G_d+l}\Gamma_U(G_d+l,x/b_I)/\Gamma(G_d+l)\end{aligned} \tag{12}$$

Authorized licensed use limited to: Princeton University. Downloaded on May 27,2022 at 01:57:22 UTC from IEEE Xplore. Restrictions apply.

at the RX is given by

$$\gamma_{B,\mathrm{JT}} = \rho\Big(\sum_{k=1}^{K_1}\mathbb{I}_{1,k}\alpha_{1,k}\|\boldsymbol{h}_{1,k}\|^2 + \sum_{k=1}^{K_2}\mathbb{I}_{2,k}\alpha_{2,k}\|\boldsymbol{h}_{2,k}\|^2\Big) = \gamma_{B,\mathrm{JT},1} + \gamma_{B,\mathrm{JT},2} = \rho_{B,s}/\sigma_z^2 \quad (19)$$

where $\gamma_{B,\mathrm{JT},i} \triangleq \rho\sum_{k=1}^{K_2}\mathbb{I}_{i,k}\alpha_{i,k}\|\boldsymbol{h}_{i,k}\|^2$ with $\rho \triangleq P_T/\sigma_z^2$ and $\rho_{B,s} = P_T\big(\sum_{k=1}^{K_1}\mathbb{I}_{1,k}\alpha_{1,k}\|\boldsymbol{h}_{1,k}\|^2 + \sum_{k=1}^{K}\mathbb{I}_{2,k}\alpha_{2,k}\|\boldsymbol{h}_{2,k}\|^2\big)$.

Proof: The derivation steps are similar to the proof of *Theorem 1*. ∎

Theorem 6: Assuming unreliable main and secondary backhaul connections, the under-populated MC-dRRUS results in an SNR, $\gamma_{B,\mathrm{JT}}$, that is distributed according to the summation of gamma functions. The MGF is given by

$$M_{B,\gamma_{\mathrm{JT}}}(s) = \overline{\sum}_{l_1}\overline{\sum}_{l_2}\prod_{j=1}^{K_1+K_2}(s+\tilde{\beta}_j)^{-l_jN_j} \quad (20)$$

where $\overline{\sum}_{l_1} \triangleq \sum_{l_{11}=0}^{1}\cdots\sum_{l_{1K_1}=0}^{1}\prod_{j=1}^{K_1}\big((1-R_{1,k})^{1-l_{1j}}(R_{1,j}/\tilde{\alpha}_{1,j}^{N_{1,j}})^{l_{1j}}\big)$, $\overline{\sum}_{l_2} \triangleq \sum_{l_{21}=0}^{1}\cdots\sum_{l_{2K_2}=0}^{1}\prod_{j=1}^{K_2}\big((1-R_{2,k})^{1-l_{2j}}(R_{2,j}/\tilde{\alpha}_{2,j}^{N_{2,j}})^{l_{2j}}\big)$, $\tilde{\beta}_j$, l_j, and N_j respectively denote the jth elements of $\tilde{\boldsymbol{\beta}} = [1/\tilde{\alpha}_{1,1},\ldots,1/\tilde{\alpha}_{1,K_1},1/\tilde{\alpha}_{2,1},\ldots,1/\tilde{\alpha}_{2,K_2}]^T$, $\boldsymbol{l} = [l_{1,1},\ldots,l_{1,K_1},l_{2,1},\ldots,l_{2,K_2}]^T$, and $\boldsymbol{N} = [N_{1,1},\ldots,N_{1,K_1},N_{2,1},\ldots,N_{2,K_2}]^T$. Additional terms specified in (20) are defined in Appendix C.

Proof: See Appendix C. ∎

A. Outage Probability and Spectral Efficiency

Having applied similar procedures to achieve an accurate and approximation of the MGF as in Section IV, the outage probability can be expressed by a finite number of upper incomplete-gamma distributions at the threshold SNR value o_{th} that causes an outage as follows:

$$OP_B(o_{\mathrm{th}}) = 1 - \overline{\sum}_{l_1}\overline{\sum}_{l_2}\sum_{l=0}^{N_{B,1}}\delta_{B,l}(b_{B,I})^{G_{B,d}} \times \Gamma_u(G_{B,d}+l, o_{\mathrm{th}}/b_{B,I})/\Gamma(G_{B,d}+l) \quad (21)$$

where $b_{B,I} \triangleq \min\big(\frac{1}{\tilde{\beta}_{B,1}},\ldots,\frac{1}{\tilde{\beta}_{B,K_1+K_2}}\big)$, $G_{B,d} \triangleq \sum_{j=1}^{K_1+K_2}N_j$, $N_{B,1}$ denotes an upper limit summation, and $\delta_{B,l} \triangleq \frac{1}{l}\sum_{i=1}^{l} ir_i\delta_{l-i}$ with $\delta_0 = 1$ and $r_i = \sum_{j=1}^{K_1+K_2}N_j(1-b_{B,I}\tilde{\beta}_{B,i})^j$.

Corollary 5: For unreliable backhaul connections, the achievable spectral efficiency of the proposed dACDD-JT scheme in MC-dRRUS is given by

$$\mathrm{SE}_B = \frac{1}{\log(2)}\overline{\sum}_{l_1}\overline{\sum}_{l_2}(b_{B,I})^{G_{B,d}}\Big[\sum_{l=0}^{N_{B,1}}\frac{\delta_{B,l}}{\Gamma(G_{B,d}+l)} \times G_{2,3}^{3,1}\big(1/b_{B,I}\big|\begin{matrix}0,1\\ G_{B,d}+l,0,0\end{matrix}\big)\Big]. \quad (22)$$

Proof: The derivation steps are similar to the proof for *Theorem 3*. ∎

B. Diversity Gain Analysis

Depending on the noise power, we can distinguish two operating regions, namely the noise dominant cooperative region at low SNRs and the backhaul reliability dominant regions at high SNRs. Specifically, we find that when the SNR increases, the proposed MC-dRRUS will leave the cooperative region, and the diversity gain is not achieved.

Corollary 6: In the backhaul reliability dominant region, the asymptotic outage probability at high SNRs is given by

$$\mathrm{OP}_B^{\mathrm{as}} = \prod_{k=1}^{K_1}(1-R_{1,k})\prod_{k=1}^{K_2}(1-R_{2,k}). \quad (23)$$

Proof: For the kth RRUs, we can compute

$$M_{B,k}(s) = M_{B,1,k}(s)M_{B,1,k}(s) = \big((1-R_{1,k}) + (R_{1,k}/\tilde{\alpha}_{1,k}^{N_{1,k}})(s+1/\tilde{\alpha}_{1,k})^{-N_{1,k}}\big) \times \big((1-R_{2,k}) + (R_{2,k}/\tilde{\alpha}_{2,k}^{N_{2,k}})(s+1/\tilde{\alpha}_{2,k})^{-N_{2,k}}\big). \quad (24)$$

As the SNR increases, $M_{B,k}(s)$ is governed by $(1-R_{1,k})$, that is, at $l_{1k} = 0$ and $l_{2k} = 0$. Thus, $M_{B,k}(s) \overset{\rho\to\infty}{\approx} = (1-R_{1,k})$. Eventually, $M_B(s) \overset{\rho\to\infty}{\approx} = \prod_{k=1}^{K_1}(1-R_{1,k})\prod_{k=1}^{K_2}(1-R_{2,k})$. ∎

Note that this is a similar observation that was analyzed in [23]. Different from [23], we observe that in the cooperative region at low SNRs, a full transmit diversity gain can be achieved via JT.

VI. Simulation Results

In this section, we present simulation results to highlight the SE and OP performance of our proposed dACDD-JT scheme for multi-cluster systems. The number of RRUs can be determined by the number of elements of $\prec a,b,c,d \succ$ that specifies its element to the RRU sequentially. Thus, a, is assigned to $\mathrm{RRU}_{j,1}$, whereas d is assigned to $\mathrm{RRU}_{j,4}$. In addition, when only one element is specified for N_js, this means that the same number of multipath elements is assumed. For link-level simulations, we separately consider the following two cases:

A. Ideal Backhaul Connections

We assume the following simulation setup.

1) C_1: Six RRUs are placed at $\prec$ $(-1.2,4.7),(0.7,4.0),(3.0,3.0),(-2.5,2.7),(-3.3,0.4),(-3.0,3.5)$ $\succ$. The first cluster master, CM_1, is placed at $(0,2)$ in a 2-D plane.

$$\mathrm{SE} = \frac{1}{\log(2)}\widehat{\sum}_{\substack{n_1,\ldots,n_M\\ n_1\neq\ldots\neq n_M}}\widetilde{\sum}_{\substack{\tilde{n}_1,\ldots,\tilde{n}_M\\ \tilde{n}_1\neq\ldots\neq\tilde{n}_M}}\prod_{k=1}^{M}(M+1-k)^{-e_k}\Gamma(e_k) \times\prod_{k=1}^{M}(M+1-k)^{-\tilde{e}_k}\Gamma(\tilde{e}_k)(b_I)^{G_d}\Big[\sum_{l=0}^{N_1}\frac{\delta_l}{\Gamma(G_d+l)}G_{2,3}^{3,1}\big(1/b_I\big|\begin{matrix}0,1\\ G_d+l,0,0\end{matrix}\big)\Big] \quad (15)$$

Authorized licensed use limited to: Princeton University. Downloaded on May 27,2022 at 01:57:22 UTC from IEEE Xplore. Restrictions apply.

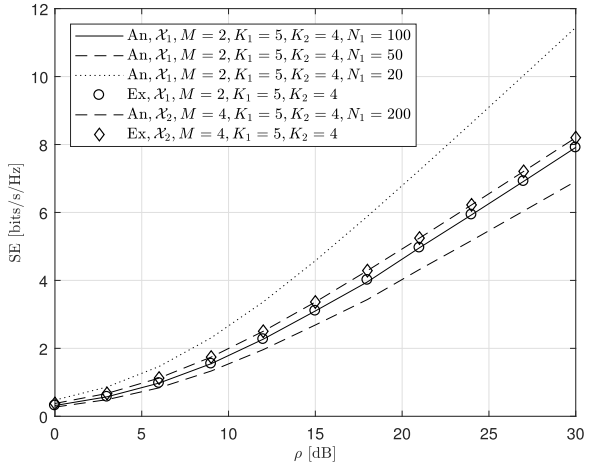

Fig. 3. SE for various system and channel parameters.

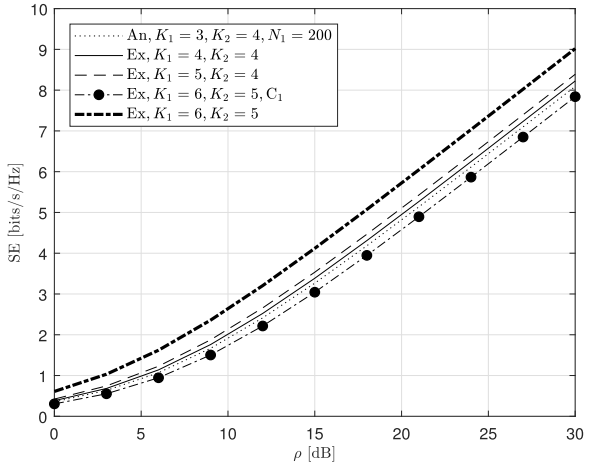

Fig. 4. SE for various over-popularities of dRRUSs with $\mathcal{X}_3$.

2) C_2: Four RRUs are placed at $\prec (12.8, 3.3), (7.4, 2.5), (10.0, 4.6), (9.0, 1.7) \succ$. The second cluster master, CM_2, is placed at $(10.0, 3.0)$ in a 2-D plane.
3) For CP-SC transmissions, we assume that $Q = 32$ and $N_{\mathrm{CP}} = 8$. Thus, the respective CM can support up to four RRUs for dACDD operation, i.e., $M = 4$.
4) RX is placed at $(3, -3)$.
5) In all the scenarios, we fix $P_T = 1$ for CP-SC transmissions. A fixed path-loss exponent is assumed to be $\epsilon = 2.09$ [38].
6) The relative time difference, $\delta T_{i,m}$, between the arrival time of the signal transmitted from $\mathrm{RRU}_{i,m}$ with respect to $\mathrm{RRU}_{i,1}$ is represented as an integer value uniformly generated between 0 and N_{CP}.

We consider several frequency selective fading channel parameters for two clusters depending on the respective number of RRUs, K_1 and K_2.

1) $\mathcal{X}_1$: $N_{1,j} =\prec 2, 3, 4, 2, 3 \succ$ and $N_{2,j} =\prec 3, 2, 3, 3 \succ$, so that $K_1 = 5$ and $K_2 = 4$.
2) $\mathcal{X}_2$: $N_{1,j} =\prec 3, 4, 2, 3, 2 \succ$ and $N_{2,j} =\prec 3, 2, 3, 3 \succ$.
3) $\mathcal{X}_3$: $N_{1,j} =\prec 2, 3, 4, 2, 3, 4 \succ$ and $N_{2,j} =\prec 3, 2, 3, 3, 4 \succ$.
4) $\mathcal{X}_4$: $N_{1,j} =\prec 2, 3, 4 \succ$ and $N_{2,j} =\prec 3, 2, 3 \succ$.
5) $\mathcal{X}_5$: $N_{1,j} =\prec 3, 4, 5, 3, 4, 5 \succ$ and $N_{2,j} =\prec 5, 4, 5, 5, 5 \succ$.
6) $\mathcal{X}_6$: $N_{1,j} =\prec 3, 4, 5, 3, 4, 5 \succ$ and $N_{2,j} =\prec 3, 2, 3, 3 \succ$.

We denote the analytically derived performance metric by **An**, whereas we denote the exact performance metric obtained by the link-level simulations by **Ex** in the sequel. Since there is no existing similar setup, i.e., CP-SC based MC-dACDD with JT, we mainly focus on the proposed scheme in this paper.

1) Verification of the Analytical Spectral Efficiency: We first verify the analytically derived spectral efficiency for two overpopulated dRRUSs. The first dRRUS with $\mathcal{X}_1$ assumes that dACDD supports two RRUs, while five and four RRUs exist in C_1 and C_2, respectively. For the second dRRUS with $\mathcal{X}_2$, dACDD supports four RRUs, while five and four RRUs exist in C_1 and C_2, respectively. For two overpopulated dRRUSs, Fig. 3 shows the accuracy of our analytically derived approximate spectral efficiency comparing with the exact spectral efficiency. This figure also shows that if N_1 is not sufficiently large, an approximation, which is derived by Corollary 3, does not provide a sufficient accuracy for the spectral efficiency. Thus, in the sequel, we assume a sufficiently large value for N_1 to ensure an accurate approximation. In general, as either K_1, or K_2, or M increases, a larger N_1 is required to obtain a very reliable approximate analytical spectral efficiency.

2) Comparisons of Spectral Efficiency With Respect to a Number of Clusters: In this simulation, we assume that $M = 4$. For the first four fading channel parameters of $\mathcal{X}_1 - \mathcal{X}_4$ with C_1 and $M = 4$, we can categorize that

- Underpopulated dRRUS ($K_1 < M$): $\mathcal{X}_4$.
- Overpopulated dRRUS ($K_1 > M$): $\mathcal{X}_1$, $\mathcal{X}_2$, and $\mathcal{X}_3$.

In contrast, the second dRRUS deployed in C_2 is full-populated with $\mathcal{X}_1$, $\mathcal{X}_2$, and $\mathcal{X}_4$, i.e., $K_2 = M$. When the dRRUS is either underpopulated or full-populated, the CMs make full use of RRUs for dACDD operation. In generating Fig. 4, we mainly use $\mathcal{X}_3$ with various over-popularity of dRRUSs. From Fig. 4 we can extract the following facts:

- As the dRRUS is populated with more RRUs, a greater SE can be achieved.
- As the number of clusters increases, a greater SE can be achieved. However, more tight restriction on the number of RRUs for dACDD exists due to different frequency selective fading severity across the deployed clusters.

3) Impact of the Number of Multipath Components and M on the SE: At a fixed 18 dB SNR, Fig. 5 shows the SE for various system and channel parameters. For underpopulated and overpopulated dRRUSs, the impact of M on the SE is investigated. This figure shows the following observations:

- For a given K_1 and K_2, as M increases, the dRRUS is populated with less RRUs. Although the SE increases in proportion to M, the growth rate of the SE decreases.
- As K_1 or K_2 increases, the growth rate of the SE increases. For example, $(K_1 = 6, K_2 = 5)$ vs. $(K_1 = 5, K_2 = 4)$.
- As the number of multipath components increases, a greater SE is achieved. For example, $\mathcal{X}_3$ vs. $\mathcal{X}_5$.

Authorized licensed use limited to: Princeton University. Downloaded on May 27,2022 at 01:57:22 UTC from IEEE Xplore. Restrictions apply.

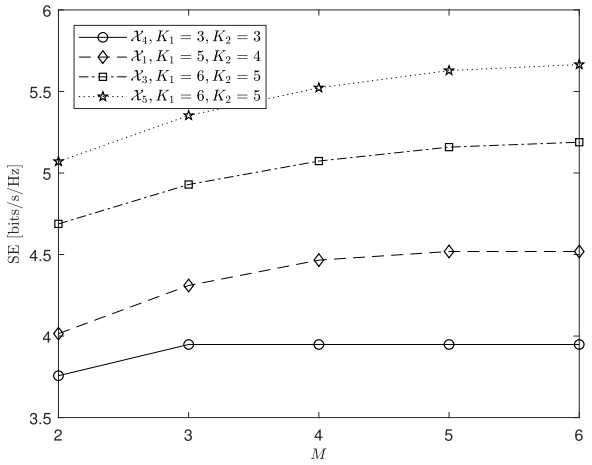

Fig. 5. SE for various values of M and different numbers of multipath components.

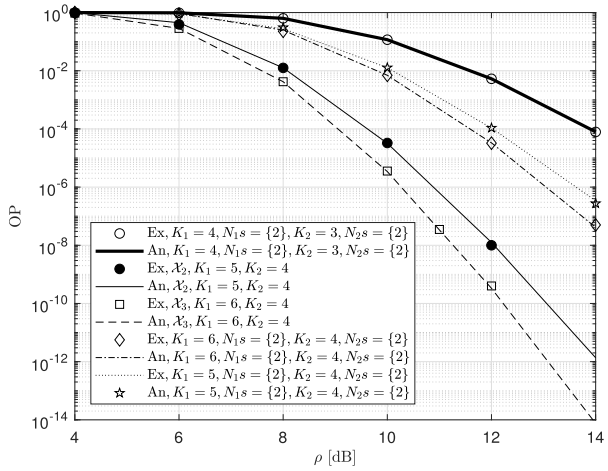

Fig. 6. OP for various values of K_1, K_2, and different numbers of multipath components.

4) Diversity Gain Analysis via the Outage Probability: For the outage probability analysis, we mainly consider the overpopulated dRRUS for C_1 and the full populated dRRUS for C_2 with $M = 4$. Due to a large diversity gain, it is hard to measure an approximate slope from the curves of the OP as either K_1 or K_2 increases. The following specific observations can be made from Fig. 6.

- The OP obtained by (16) provides a very reliable OP although it is approximated by N_1 gamma distributions.
- In general, as either K_1 or K_2 increases, a lower OP can be obtained. For example, $K_1 = 6, K_2 = 4$ vs. $K_1 = 5, K_2 = 4$.

Since the closed-form expression for the OP is based on the computation of the permanents of the matrix, it is necessary to investigate the diversity gain for a specific pair of n_js that satisfy the condition: $n_j \in \mathbb{N}_0$, with $n_j \leq K_j$ and $n_1 \neq n_2 \neq \ldots \neq n_M$. For several sets of n_js, Fig. 7 shows the following facts:

- Comparing with the OP composed by a whole set of n_js, each considered set of n_js provides the same slope as the SNR increases. Thus, this figure shows that the diversity gain is irrespective of a particular set of n_js.
- As was verified by (17), the more multipath components results in a greater diversity gain. For example, $\mathcal{X}_3$ vs. the case with $N_1s = \{2\}$ and $N_2s = \{2\}$.

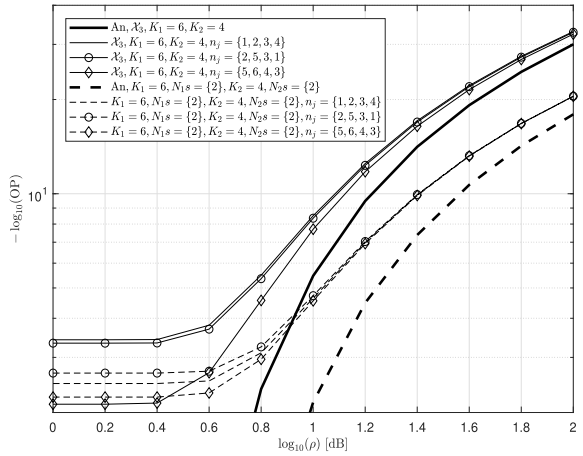

Fig. 7. OP in a $\log - \log$ axis for various pairs for the permanent matrix computation. $n_j = \{n_1, n_2, n_3, n_4\}$ for $M = 4$ denotes the set of n_js defined in (A.4).

B. Unreliable Backhaul Connections

We considered the same simulation setup as for ideal backhaul connections except for the following:

1) For CP-SC transmissions, we assume that $Q = 64$ and $N_{\mathrm{CP}} = 8$. Thus, the CMs can support up to eight RRUs for dCDD operation, i.e., $M = 8$.
2) Reliability of the main backhauls b_1 and b_2 is assumed to be 0.99.
3) Reliability of the secondary backhauls are assumed to be $R_{1,k}s =\prec 0.9, 0.95, 0.94, 0.8 \succ$ and $R_{2,k}s =\prec 0.9, 0.95, 0.94, 0.6 \succ$.

We consider several frequency selective fading channel parameters shown below for two clusters depending on the respective number of RRUs.

1) $\mathcal{Y}_1$: $N_{1,j} =\prec 2, 3, 4, 2 \succ$ and $N_{2,j} =\prec 3, 2, 3 \succ$, so that $K_1 = 4$ and $K_2 = 3$.
2) $\mathcal{Y}_2$: $N_{1,j} =\prec 2, 3, 2, 2 \succ$ and $N_{2,j} =\prec 3, 2, 3 \succ$.
3) $\mathcal{Y}_3$: $N_{1,j} =\prec 2, 3, 4 \succ$ and $N_{2,j} =\prec 3, 2, 3 \succ$.
4) $\mathcal{Y}_4$: $N_{1,j} =\prec 2, 3, 4, 3 \succ$ and $N_{2,j} =\prec 3, 2, 3, 4 \succ$.

1) Outage Probability Analysis: From Fig. 8, we first verify the analytically derived OPs for various numbers of RRUs and channel parameters. This figure shows that the analytically derived OPs match closely with the exact link-level simulations for underpopulated dRRUS. This figure also shows that if $N_{1,B}$ is sufficiently large, the outage approximation proposed by (21), reliably approximates the simulation results. For scenario $\mathcal{Y}_3$, we compare the OP of the dRRUS with two clusters with that of a single cluster. The figure shows that the use of two clusters results in a lower OP for dCDD-JT in both the cooperative and backhaul reliability dominant regions when the reliabilities are similar for the secondary backhaul connections.

Authorized licensed use limited to: Princeton University. Downloaded on May 27,2022 at 01:57:22 UTC from IEEE Xplore. Restrictions apply.

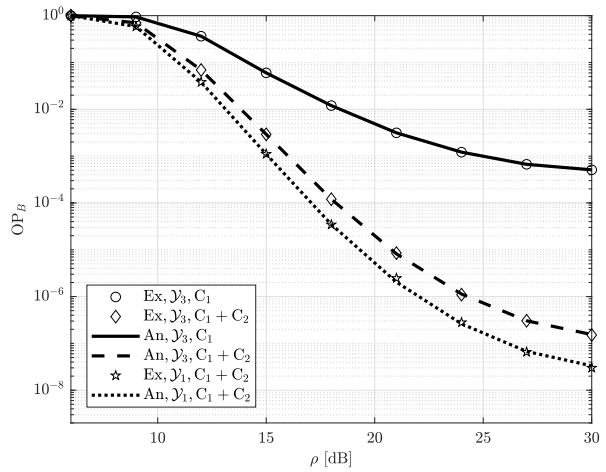

Fig. 8. OP for various system and channel parameters and unreliable backhaul connections.

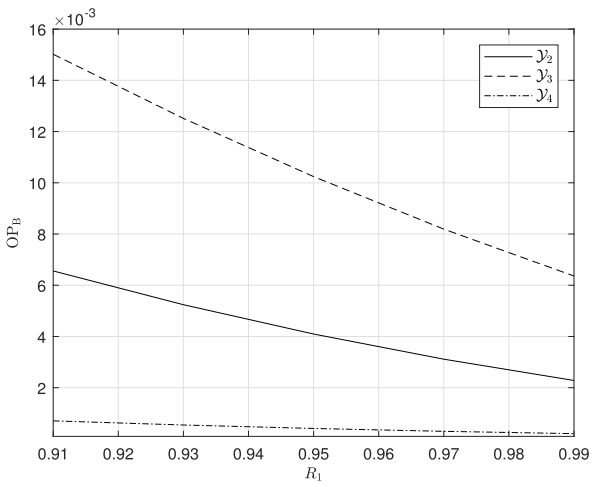

Fig. 10. Impact of main backhaul reliability on OP.

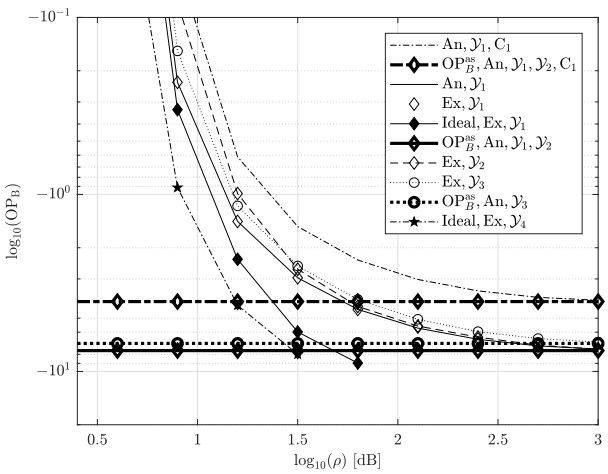

Fig. 9. OP for various scenarios and unreliable backhaul connections.

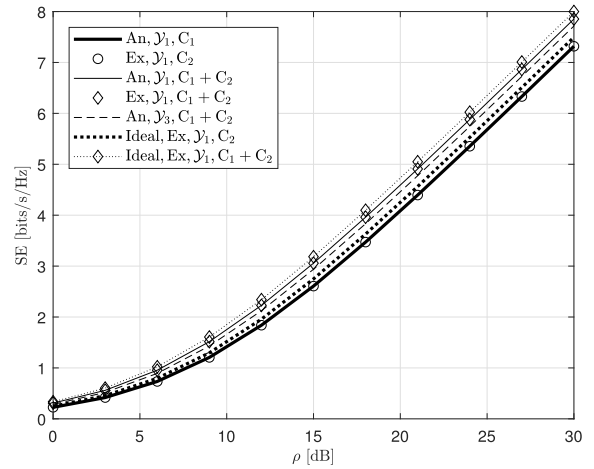

Fig. 11. SE with ideal backhaul and non-ideal backhaul connections.

In Fig. 9, we plot the OP in terms of $-\log_{10}(\mathrm{OP}_B)$ to investigate the impact of backhaul reliability on the asymptotic OP at high SNRs. We also plot the OP with ideal backhaul connections and the asymptotic lower bound on the OP. From Figs. 8 and 9, we can extract the following facts:

- As the dRRUS is populated with more RRUs, a lower OP can be achieved when backhaul reliabilities are similar and the number of multipath components are similar.
- As the number of clusters increases, a lower OP can be achieved.
- Diversity gain can be observed only in the cooperative region. As the SNR increases, MC-dRRUS leaves the cooperative region, so that backhaul reliability tends to determine the lower bound on the OP.
- When only one cluster exists in the system, the asymptotic OP is given by $\mathrm{OP}_B^{\mathrm{as}} = \prod_{k=1}^{K_1}(1 - R_{1,k})$. Thus, in general, for larger number of clusters, a lower bound on $\mathrm{OP}_B^{\mathrm{as}}$ is obtained when backhauls are relatively reliable.

At 15 dB SNR, Fig. 10 shows the impact of improving the reliability of the main backhaul, b_1, on the OP. Other backhauls are assumed to have the same reliability as specified in the scenarios. This figure shows that the main backhaul exerts a stronger influence over less populated dRRUSs than on more populated dRRUSs since the backhaul reliability is the product of the main and secondary backhaul reliability.

2) Spectral Efficiency: Fig. 11 shows the SE with ideal backhaul and non-ideal backhaul connections. For scenario $\mathcal{Y}_1$, this figure shows that ideal backhaul connections result in a greater SE. In addition, as the number of clusters increases, a greater spectral efficiency can be obtained. Especially, at 15 dB SNR, the use of two clusters for scenario $\mathcal{Y}_1$ provides 0.5 bits/s/Hz greater spectral efficiency than a single cluster. Furthermore, a greater population of each dRRUS results in a greater spectral efficiency.

VII. Conclusion

In this paper, we have proposed a multiple cluster-based transmit diversity scheme for asynchronous joint transmissions in local and private wireless networks. To relax the requirement of full channel state information at the private network server and deal with different propagation over the paths of the distributed systems composed of remote radio units, a dACDD scheme has been developed for multiple clusters deployed

Authorized licensed use limited to: Princeton University. Downloaded on May 27,2022 at 01:57:22 UTC from IEEE Xplore. Restrictions apply.

in the local and private wireless networks. We consider a multi-level hierarchical PTP to break the dependency of different dRRUS clusters from a common PNS allowing each dRRUS cluster to use dACDD independently from another dACDD cluster. For i.n.i.d. frequency selective fading channels, a new closed-form expression for the spectral efficiency has been derived. Its accuracy has been also verified compared with link-level simulations. By integrating a multiple single carrier transmission scheme, propagation delay estimation, and operation at the remote radio units effectively, we have seen that the proposed multiple cluster-based asynchronous joint transmissions can achieve the desired spectral efficiency for various simulations scenarios. We have also shown that backhaul reliability is a key constraint to maintain the target performance especially at high SNRs. Due to backhaul reliability, we have found that the MC-dRRUS displays two distinctive operating regions, namely, the cooperative region and the backhaul reliability dominant region. Their existence has been verified theoretically and numerically. We have confirmed that careful design of the MC-dRRUS to remain within the cooperative region, will result in reaping the full transmit diversity gains of joint transmission without requiring full channel state information.

APPENDIX A: PROOF OF THEOREM 2

To simplify the notation, let us define x_m as $x_m \triangleq \rho\alpha_{1,\langle K_1-M+m\rangle}\|\boldsymbol{h}_{1,\langle K_1-M+m\rangle}\|^2$. Note that the order statistics are implicitly involved in this definition. We mainly focus on the derivation of the distribution for $\gamma_{\mathrm{JT},1}$ in the sequel. The MGF of $\gamma_{\mathrm{JT},1}$ can be defined as (A.1) provided at the bottom of the next page. In (A.1), $\mathrm{Per}(\boldsymbol{A}_{\max}^{K_1,M})$ denotes the permanents of the matrix [39] defined as follows:

$$\boldsymbol{A}_{\max}^{K_1,M} \triangleq X_c \begin{bmatrix} F_1(x_1) & f_1(x_1) & \cdots & f_1(x_M) \\ F_2(x_1) & f_2(x_1) & \cdots & f_2(x_M) \\ \vdots & \vdots & \vdots & \vdots \\ F_{K_1}(x_1) & f_{K_1}(x_1) & \cdots & f_{K_1}(x_M) \\ \underbrace{K_1-M} & \underbrace{1} & \underbrace{1} & \underbrace{1} \end{bmatrix} \tag{A.2}$$

with $X_c \triangleq \frac{1}{(K_1-M)!}$, and $\left[\underbrace{\boldsymbol{a}_1}_{i} \underbrace{\boldsymbol{a}_2}_{j}\right]$ denoting i copies of $\boldsymbol{a}_1$ and j copies of $\boldsymbol{a}_2$. In addition, $F_j(x_1)$ and $f_j(x_i)$ are respective defined as follows:

$$\begin{aligned} F_j(x_1) &= \frac{\gamma_l(N_{1,\langle K_1-M+m\rangle}, 1/\rho\alpha_{1,\langle K_1-M+m\rangle}x_1)}{\Gamma(N_{1,\langle K_1-M+m\rangle})} \\ f_j(x_i) &= (\rho\alpha_{1,\langle K_1-M+j\rangle})^{-N_{1,\langle K_1-M+j\rangle}} e^{-1/\rho\alpha_{1,\langle K_1-M+j\rangle}x_i} \\ &\quad (x_i)^{N_{1,\langle K_1-M+j\rangle}-1}/\Gamma(N_{1,\langle K_1-M+j\rangle}) \end{aligned} \tag{A.3}$$

where $\gamma_l(\cdot,\cdot)$ denotes the incomplete lower-gamma function. Thus, $[\cdot]_{J_6}$ can be expressed as:

$$\begin{aligned} [\cdot]_{J_6} = \sum\nolimits_{\substack{n_1,\ldots,n_M \\ n_1\neq n_2\neq\ldots\neq n_M}}^{K_1} \prod\nolimits_{i=1}^{M} (b_i)^{p_i}(x_i)^{p_i-1}e^{-(s+b_i)x_i}/\Gamma(p_i) \\ \times \prod\nolimits_{i=M+1}^{K_1} \gamma_l(p_i, b_i x_1)/\Gamma(p_i) \end{aligned} \tag{A.4}$$

where we simplify the notation by defining $p_i \triangleq N_{1,\langle K_1-M+n_i\rangle}$, and $b_i \triangleq 1/\rho\alpha_{1,\langle K_1-M+n_i\rangle}$. Next, we rewrite $\gamma(p_i, b_i x_1)/\Gamma(p_i)$ as follows:

$$\begin{aligned} \frac{\gamma(p_i, b_i x_1)}{\Gamma(p_i)} &= \sum\nolimits_{a_{i,1}+a_{i,2}+\ldots+a_{i,p_i+1}=1} \binom{1}{a_{i,1},a_{i,2},\ldots,a_{i,p_i+1}} \\ &\quad (-1)^{\lambda_i}(b_i)^{\tilde{p}_i} x_1^{\tilde{p}_i} e^{-\lambda_i b_i x_1}/\theta_i \\ &= \sum\nolimits_{\mathrm{sum}(\boldsymbol{a}_{i,p_i+1})=1} \binom{1}{\boldsymbol{a}_{i,p_i+1}} X_i x_1^{\tilde{p}_i} e^{-\lambda_i b_i x_1} \end{aligned} \tag{A.5}$$

where $\lambda_i \triangleq \sum_{j=2}^{p_i+1} \boldsymbol{a}_i(j)$, $\theta_i \triangleq \prod_{j=2}^{p_i}(\Gamma(j))^{\boldsymbol{a}_i(j+1)}$, $\tilde{p}_i \triangleq \sum_{j=3}^{p_i+1}(j-2)\boldsymbol{a}_i(j)$, and $X_i \triangleq (-1)^{\lambda_i}(b_i)^{\tilde{p}_i}/\theta_i$ for $\boldsymbol{a}_i$'s. Thus, we can evaluate (A.4) as (A.6) provided at the bottom of the next page. In (A.6), we have defined $A_{M,1} \triangleq \prod_{i=1}^{M} \frac{(b_i)^{p_i}}{\Gamma(p_i)}$. Now replacing x_i with $x_i = \sum_{j=1}^{i} y_j$, where $\{y_1,\ldots,y_N\}$ are the spacing statistics of the order statistics, $\{x_1,\ldots,x_M\}$, $[\cdot]_{J_7}$ can be expressed as (A.7). In the derivation of (A.7), the multinomial and binomial theorems are used in the derivation. Now using the spacing statistics, $\{y_i\}$ becomes independent, so that (A.1) is computed as follows:

$$\begin{aligned} M_{\gamma_{\mathrm{JT},1}}(s) = \widehat{\sum}_{\substack{n_1,\ldots,n_M \\ n_1\neq n_2\neq\ldots\neq n_M}} \prod\nolimits_{k=1}^{M} (M+1-k)^{-e_k}\Gamma(e_k) \\ \times \prod\nolimits_{k=1}^{M} (s+q_k)^{-e_k} \end{aligned} \tag{A.8}$$

where $\widehat{\sum}_{\substack{n_1,\ldots,n_M \\ n_1\neq n_2\neq\ldots\neq n_M}}$ is given by (A.9) provided at the bottom of the next page. Additional terms are defined as follows: $e_1 \triangleq p_1 + \sum_{j=2}^{M} \boldsymbol{a}_j(1) + \sum_{j=M+1}^{K_1} \tilde{p}_j$, $e_{k\geq 2} \triangleq \sum_{j=2}^{M} \boldsymbol{a}_j(k) + 1$, $q_1 \triangleq \frac{1}{M}\big(\sum_{j=1}^{M} b_j + \sum_{j=M+1}^{K_1} \lambda_j b_j\big)$, and $q_{k\geq 2} \triangleq \frac{1}{M+1-k}\big(\sum_{j=k}^{M} b_j\big)$.

With an assumption that M RRUs, out of K_2 RRUs, are selected by CM_2, the MGF of $\gamma_{\mathrm{JT},2}$ is derived as follows:

$$\begin{aligned} M_{\gamma_{\mathrm{JT},2}}(s) = \widetilde{\sum}_{\substack{\tilde{n}_1,\ldots,\tilde{n}_M \\ \tilde{n}_1\neq\tilde{n}_2\neq\ldots\neq\tilde{n}_M}} \prod\nolimits_{k=1}^{M} (M+1-k)^{-\tilde{e}_k}\Gamma(\tilde{e}_k) \\ \times \prod\nolimits_{k=1}^{M} (s+\tilde{q}_k)^{-\tilde{e}_k} \end{aligned} \tag{A.10}$$

where $\widetilde{\sum}_{\substack{\tilde{n}_1,\ldots,\tilde{n}_M \\ \tilde{n}_1\neq\tilde{n}_2\neq\ldots\neq\tilde{n}_M}}$ is defined by (A.11), provided at the bottom of the next pages. For $\hat{p}_i \triangleq N_{2,\langle K_2-M+\tilde{n}_i\rangle}$, $\hat{b}_i \triangleq \frac{1}{\rho\alpha_{2,\langle K_2-M+\tilde{n}_i\rangle}}$, $A_{M_2} \triangleq \prod_{i=1}^{M}(\hat{b}_i)^{\hat{p}_i}/\Gamma(\hat{p}_i)$, $\hat{\lambda}_i \triangleq \sum_{j=2}^{\hat{p}_i+1} \hat{\boldsymbol{a}}_i(j)$, $\hat{\theta}_i \triangleq \prod_{j=2}^{\hat{p}_i}(\Gamma(j))^{\tilde{\boldsymbol{a}}_i(j+1)}$, $\hat{\tilde{p}}_i \triangleq \sum_{j=3}^{\hat{p}_i+1}(j-2)\tilde{\boldsymbol{a}}_i(j)$, and $\hat{X}_i \triangleq (-1)^{\hat{\lambda}_i}(\hat{b}_i)^{\hat{\tilde{p}}_i}/\hat{\theta}_i$ for $\tilde{\boldsymbol{a}}_i$s. $\tilde{e}_k$ and $\tilde{q}_k$ are defined as those of e_k and q_k. Since the SNR realized at the RX is the sum of two RVs, $\gamma_{\mathrm{JT},1}$ and $\gamma_{\mathrm{JT},2}$, the MGF is given by (10).

APPENDIX B: PROOF OF THEOREM 4

For a particular pair of n_is, as $b_M \to 0$, we compute (A.1) based on (A.4) as follows:

$$\begin{aligned} &\frac{(b_M)^{p_M}}{\Gamma(p_M)} \int_{x_{M-1}}^{\infty} (x_M)^{P_M-1} e^{-(s+b_M)x_M} dx_M \\ &\quad \approx (b_M)^{p_M}(s)^{-p_M} e^{-(s)x_{M-1}} \\ &\qquad \times \sum\nolimits_{l_M=0}^{P_M-1} (s)^{l_M}/(l_M!)(x_{M-1})^{l_M}. \end{aligned} \tag{B.1}$$

Authorized licensed use limited to: Princeton University. Downloaded on May 27,2022 at 01:57:22 UTC from IEEE Xplore. Restrictions apply.

Having applied sequential computations, and using an approximation, $\lim_{x\to 0}\gamma_l(n,x)=\frac{x^n}{n}$, (A.4) can be computed as (B.2) provided at the bottom of the page. Thus, at a given outage SNR, $\mathrm{o_{th}}$, the asymptotic outage probability is given by (B.3). Note that (B.3) shows that the diversity gain $G_{d,C_1}=\sum_{i=1}^{K_1}N_{1,i}$ can be achieved in the asymptotic high SNR region independent of a particular pairs of n_i.

Appendix C: Proof of Theorem 6

To simplify the notation, let us define x_k as $x_k\triangleq\rho\alpha_{1,k}\mathbb{I}_{1,k}\|\boldsymbol{h}_{1,k}\|^2\triangleq\tilde{\alpha}_{1,k}\mathbb{I}_{1,k}\|\boldsymbol{h}_{1,k}\|^2$. According to a Bernoulli process, the PDF of x_k is given by [23]

$$f_{x_k}(x)=(1-R_{1,k})\delta(x)+\frac{R_{1,k}e^{-x/\tilde{\alpha}_{1,k}}x^{N_{1,k}-1}(\tilde{\alpha}_{1,k})^{-N_{1,k}}}{\Gamma(N_{1,k})} \tag{C.1}$$

where $\delta(x)$ denotes the Dirac delta function. Based on the PDF, the MGF is given by

$$\begin{aligned}M_{1,k}(s)&=(1-R_{1,k})+(R_{1,k}/\tilde{\alpha}_{1,k}^{N_{1,k}})(s+1/\tilde{\alpha}_{1,k})^{-N_{1,k}}\\&=\sum\nolimits_{l_{1k}=0}^{1}(1-R_{1,k})^{1-l_{1k}}(R_{1,k}/\tilde{\alpha}_{1,k}^{N_{1,k}})^{l_{1k}}\\&\quad\times(s+1/\tilde{\alpha}_{1,k})^{-l_{1k}N_{1,k}}\end{aligned} \tag{C.2}$$

$$M_{\gamma_{\mathrm{JT},1}}(s)=\int_0^\infty\int_{x_1}^\infty\cdots\int_{x_{M-2}}^\infty\int_{x_{M-1}}^\infty\left[e^{-s(\sum_{j=1}^M x_j)}\mathrm{Per}(\boldsymbol{A}_{\max}^{K_1,M})\right]_{J_6}dx_M\ldots dx_2dx_1 \tag{A.1}$$

$$\begin{aligned}[\cdot]_{J_6}=&\sum_{\substack{n_1,\ldots,n_M\\ n_1\neq n_2\neq\ldots\neq n_M}}A_{M,1}\sum\nolimits_{\mathrm{sum}(\boldsymbol{a}_{M+1,p_{M+1}+1})=1}\cdots\sum\nolimits_{\mathrm{sum}(\boldsymbol{a}_{K_1,p_{K_1}+1})=1}\binom{1}{\boldsymbol{a}_{M+1,p_{M+1}+1}}\ldots\binom{1}{\boldsymbol{a}_{K_1,p_{K_1}+1}}(\prod\nolimits_{i=M+1}^{K_1}X_i)\\&\left[(x_1)^{p_1+\tilde{p}_{M+1}+\ldots+\tilde{p}_{K_1}-1}e^{-(s+b_1+\lambda_{M+1}b_{M+1}+\ldots+\lambda_{K_1}b_{K_1})y_1}(x_2)^{p_2-1}e^{-(s+b_2)x_2}\ldots(x_M)^{p_M-1}e^{-(s+b_M)x_M}\right]_{J_7}\end{aligned} \tag{A.6}$$

$$\begin{aligned}[\cdot]_{J_7}=&\sum\nolimits_{\mathrm{sum}(\boldsymbol{a}_{2,p_2})=p_2-1}\cdots\sum\nolimits_{\mathrm{sum}(\boldsymbol{a}_{M,p_M})=p_M-1}\binom{p_2-1}{\boldsymbol{a}_{2,p_2}}\ldots\binom{p_M-1}{\boldsymbol{a}_{M,p_M}}(y_1)^{p_1+\sum_{j=2}^M a_{j,1}+\tilde{p}_{M+1}+\ldots+\tilde{p}_{K_1}-1}\\&e^{-(Ms+\sum_{j=1}^M b_j+\sum_{j=M+1}^{K_1}\lambda_j b_j)y_1}(y_2)^{\sum_{j=2}^M a_{j,2}}e^{-((M-1)s+\sum_{j=2}^{K_1}b_j)y_2}\ldots(y_M)^{a_{M,M}}e^{-(s+b_M)y_M}\end{aligned} \tag{A.7}$$

$$\begin{aligned}\widehat{\sum}_{\substack{n_1,\ldots,n_M\\ n_1\neq n_2\neq\ldots\neq n_M}}\triangleq&\sum\nolimits_{\substack{n_1,\ldots,n_M\\ n_1\neq n_2\neq\ldots\neq n_M}}^{K_1}A_{M_1}\sum\nolimits_{\mathrm{sum}(\boldsymbol{a}_{M+1,p_{M+1}+1})=1}\cdots\sum\nolimits_{\mathrm{sum}(\boldsymbol{a}_{K_1,p_{K_1}+1})=1}[\prod\nolimits_{j=M+1}^{K_1}\binom{1}{\boldsymbol{a}_{j,p_j+1}}]\\&[\prod\nolimits_{i=M+1}^{K_1}X_i]\sum\nolimits_{\mathrm{sum}(\boldsymbol{a}_{2,p_2})=p_2-1}\cdots\sum\nolimits_{\mathrm{sum}(\boldsymbol{a}_{M,p_M})=p_M-1}[\prod\nolimits_{j=2}^{M}\binom{p_j-1}{\boldsymbol{a}_{j,p_j}}]\end{aligned} \tag{A.9}$$

$$\begin{aligned}\widetilde{\sum}_{\substack{\tilde{n}_1,\ldots,\tilde{n}_M\\ \tilde{n}_1\neq\tilde{n}_2\neq\ldots\neq\tilde{n}_M}}\triangleq&\sum_{\substack{\tilde{n}_1,\ldots,\tilde{n}_M\\ \tilde{n}_1\neq\tilde{n}_2\neq\ldots\neq\tilde{n}_M}}^{K_2}A_{M_2}\sum\nolimits_{\mathrm{sum}(\tilde{\boldsymbol{a}}_{M+1,p_{M+1}+1})=1}\cdots\sum\nolimits_{\mathrm{sum}(\tilde{\boldsymbol{a}}_{K_2,p_{K_2}+1})=1}[\prod\nolimits_{j=M+1}^{K_2}\binom{1}{\tilde{\boldsymbol{a}}_{j,p_j+1}}]\\&[\prod\nolimits_{i=M+1}^{K_2}\tilde{X}_i]\sum\nolimits_{\mathrm{sum}(\tilde{\boldsymbol{a}}_{2,p_2})=p_2-1}\cdots\sum\nolimits_{\mathrm{sum}(\tilde{\boldsymbol{a}}_{M,p_M})=p_M-1}[\prod\nolimits_{j=2}^{M}\binom{p_j-1}{\tilde{\boldsymbol{a}}_{j,p_j}}]\end{aligned} \tag{A.11}$$

$$\begin{aligned}[\cdot]_{J_6}^{\mathrm{as}}\propto&(\prod\nolimits_{j=1}^{M-1}\frac{1}{\Gamma(p_j)})(\prod\nolimits_{i=M+1}^{K_1}\frac{1}{\Gamma(p_i+1)})\sum\nolimits_{l_M=0}^{p_M-1}\sum\nolimits_{l_{M-1}=0}^{l_M+p_{M-1}-1}\cdots\sum\nolimits_{l_2=0}^{l_3+p_2-1}(\prod\nolimits_{j=3}^{M}\Gamma(l_j+p_{j-1}))\\&\Gamma\big(l_2+p_1+\sum\nolimits_{i=M+1}^{K_1}p_i\big)(M+1)^{(l_2+p_1+\sum_{i=M+1}^{K_1}p_i)}(\prod\nolimits_{j=2}^{M}(2+M-j)^{-l_j-p_{j-1}+l_{j-1}})\\&(\prod\nolimits_{i=1}^{K_1}(\alpha_{1,i})^{-N_{1,i}})(\rho)^{-(\sum_{i=1}^{K_1}N_{1,i})}s^{-(\sum_{i=1}^{K_1}N_{1,i})}\end{aligned} \tag{B.2}$$

$$\begin{aligned}\mathrm{OP}^{\mathrm{as}}\propto&(\prod\nolimits_{j=1}^{M-1}\frac{1}{\Gamma(p_j)})(\prod\nolimits_{i=M+1}^{K_1}\frac{1}{\Gamma(p_i+1)})\sum\nolimits_{l_M=0}^{p_M-1}\sum\nolimits_{l_{M-1}=0}^{l_M+p_{M-1}-1}\cdots\sum\nolimits_{l_2=0}^{l_3+p_2-1}\\&(\prod\nolimits_{j=3}^{M}\Gamma(l_j+p_{j-1}))\Gamma\big(l_2+p_1+\sum\nolimits_{i=M+1}^{K_1}p_i\big)(M+1)^{(l_2+p_1+\sum_{i=M+1}^{K_1}p_i)}\\&(\prod\nolimits_{j=2}^{M}(2+M-j)^{-l_j-p_{j-1}+l_{j-1}})(\prod\nolimits_{i=1}^{K_1}(\alpha_{1,i})^{-N_{1,i}})\frac{(\rho/\mathrm{o_{th}})^{-G_{d,C_1}}}{\Gamma(\sum_{i=1}^{K_1}N_{1,i}+1)}\end{aligned} \tag{B.3}$$

Authorized licensed use limited to: Princeton University. Downloaded on May 27,2022 at 01:57:22 UTC from IEEE Xplore. Restrictions apply.

$$M_{B,\gamma_{\mathrm{JT},1}}(s) = \sum_{l_{11}=0}^{1} \cdots \sum_{l_{1K_1}=0}^{1} \prod_{j=1}^{K_1} \left((1-R_{1,k})^{1-l_{1j}} (R_{1,j}/\tilde{\alpha}_{1,j}^{N_{1,j}})^{l_{1j}}\right) \prod_{j=1}^{K_1} (s+1/\tilde{\alpha}_{1,j})^{-l_{1j}N_{1,j}}$$
$$= \overline{\sum}_{l_1} \prod_{j=1}^{K_1} (s+1/\tilde{\alpha}_{1,j})^{-l_{1j}N_{1,j}} \quad \text{(C.3)}$$

where the binomial theorem is used in the final expression. According to (C.2), the MGF of $\gamma_{B,\mathrm{JT},1}$ is given by (C.3) provided at the top of the page.

With an assumption that K_2 RRUs are selected by CM_2, the MGF of $\gamma_{B,\mathrm{JT},2}$ is given by

$$M_{B,\gamma_{\mathrm{JT},2}}(s) = \overline{\sum}_{l_2} \prod_{j=1}^{K_2} (s+1/\tilde{\alpha}_{2,j})^{-l_{2j}N_{2,j}}. \quad \text{(C.4)}$$

Since the SNR realized at the RX is the sum of two RVs, $\gamma_{B,\mathrm{JT},1}$ and $\gamma_{B,\mathrm{JT},2}$, the MGF is given by $M_{B,\gamma_{\mathrm{JT}}}(s) = M_{B,\gamma_{\mathrm{JT},1}}(s) M_{B,\gamma_{\mathrm{JT},2}}(s)$.

REFERENCES

[1] K. J. Kim, H. Liu, P. L. Yeoh, P. V. Orlik, and H. V. Poor, "Backhaul reliability analysis on cluster-based transmit diversity schemes in private networks," in *Proc. IEEE Global Commun. Conf.*, Taipei, Taiwan, Dec. 2020, pp. 1–6.

[2] K. J. Kim, J. Guo, P. V. Orlik, Y. Nagai, and H. V. Poor, "A cluster-based transmit diversity scheme for asynchronous joint transmissions in private networks," in *Proc. IEEE Int. Conf. Commun.*, Montreal, QC, Canada, Jun. 2021, pp. 1–6.

[3] T. O. Olwal, K. Djouani, and A. M. Kurien, "A survey of resource management toward 5G radio access networks," *IEEE Commun. Surveys Tuts.*, vol. 18, no. 3, pp. 1656–1686, 3rd Quart., 2016.

[4] H. Li, J. Hajipour, A. Attar, and V. Leung, "Efficient HetNet implementation using broadband wireless access with fiber-connected massively distributed antennas architecture," *IEEE Wireless Commun.*, vol. 18, no. 3, pp. 72–78, Jun. 2011.

[5] J. Park, E. Song, and W. Sung, "Capacity analysis for distributed antenna systems using cooperative transmission schemes in fading channels," *IEEE Trans. Wireless Commun.*, vol. 8, no. 2, pp. 586–592, Feb. 2009.

[6] X. Zhang, Y. Sun, X. Chen, S. Zhou, J. Wang, and N. B. Shroff, "Distributed power allocation for coordinated multipoint transmissions in distributed antenna systems," *IEEE Trans. Wireless Commun.*, vol. 12, no. 5, pp. 2281–2291, May 2013.

[7] W. Feng, Y. Wang, N. Ge, J. Lu, and J. Zhang, "Virtual MIMO in multi-cell distributed antenna systems: Coordinated transmissions with large-scale CSIT," *IEEE J. Sel. Areas Commun.*, vol. 31, no. 10, pp. 2067–2081, Oct. 2013.

[8] J. Wu, J. Liu, W. Li, and X. You, "Low-complexity power allocation for energy efficiency maximization in DAS," *IEEE Commun. Lett.*, vol. 19, no. 6, pp. 925–928, Jun. 2015.

[9] X. Li, X. Ge, X. Wang, J. Cheng, and V. C. M. Leung, "Energy efficiency optimization: Joint antenna-subcarrier-power allocation in OFDM-DASs," *IEEE Trans. Wireless Commun.*, vol. 15, no. 11, pp. 7470–7483, Nov. 2016.

[10] M.-L. Tham, S. F. Chien, D. W. Holtby, and S. Alimov, "Energy-efficient power allocation for distributed antenna systems with proportional fairness," *IEEE Trans. Green Commun. Netw.*, vol. 1, no. 2, pp. 145–157, Jun. 2017.

[11] R. Heath, S. Peters, Y. Wang, and J. Zhang, "A current perspective on distributed antenna systems for the downlink of cellular systems," *IEEE Commun. Mag.*, vol. 51, no. 4, pp. 161–167, Apr. 2013.

[12] V. Nikolopoulos, M. Fiacco, S. Stavrou, and S. R. Saunders, "Narrowband fading analysis of indoor distributed antenna systems," *IEEE Antennas Wireless Propag. Lett.*, vol. 2, pp. 89–92, 2003.

[13] Q. Wu, X. Ding, and A. Chen, "A broadband dipole antenna for multi-service indoor distributed antenna system (MS-IDAS)," *IEEE Antennas Wireless Propag. Lett.*, vol. 14, pp. 839–842, 2015.

[14] K. J. Kim, M. Di Renzo, H. Liu, P. V. Orlik, and H. V. Poor, "Performance analysis of distributed single carrier systems with distributed cyclic delay diversity," *IEEE Trans. Commun.*, vol. 65, no. 12, pp. 5514–5528, Dec. 2017.

[15] X. Tao, X. Xu, and Q. Cui, "An overview of cooperative communications," *IEEE Commun. Mag.*, vol. 50, no. 6, pp. 65–71, Jun. 2012.

[16] V. Garcia, Y. Zhou, and J. Shi, "Coordinated multipoint transmission in dense cellular networks with user-centric adaptive clustering," *IEEE Trans. Wireless Commun.*, vol. 13, no. 8, pp. 4297–4308, Aug. 2014.

[17] H. Zhuang, L. Dai, L. Xiao, and Y. Yao, "Spectral efficiency of distributed antenna system with random antenna layout," *Electron. Lett.*, vol. 39, no. 6, pp. 495–496, Mar. 2003.

[18] S. Lagen, A. Agustin, and J. Vidal, "Distributed inter-cluster interference management for CoMP-based cellular networks," in *Proc. IEEE Global Commun. Conf.*, Atlanta, GA, USA, Dec. 2013, pp. 4204–4209.

[19] A. Mahmood, M. I. Ashraf, M. Gidlund, and J. Torsner, "Over-the-air time synchronization for URLLC: Requirements, challenges and possible enablers," in *Proc. 15th Int. Symp. Wireless Commun. Syst. (ISWCS)*, Lisbon, Portugal, Aug. 2018, pp. 1–6.

[20] H. Jung and I.-H. Lee, "Outage analysis of millimeter-wave wireless backhaul in the presence of blockage," *IEEE Commun. Lett.*, vol. 20, no. 11, pp. 2268–2271, Nov. 2016.

[21] Z. Mayer, J. Li, A. Papadogiannis, and T. Svensson, "On the impact of control channel reliability on coordinated multi-point transmission," *EURASIP J. Wireless Commun. Netw.*, vol. 2014, no. 1, pp. 1–16, Dec. 2014.

[22] M. M. Aldosari and K. A. Hamdi, "Energy efficiency of distributed antenna systems using fractional frequency reuse," *IEEE Commun. Lett.*, vol. 19, no. 11, pp. 1985–1988, Nov. 2015.

[23] K. J. Kim, T. A. Khan, and P. V. Orlik, "Performance analysis of cooperative systems with unreliable backhauls and selection combining," *IEEE Trans. Veh. Technol.*, vol. 66, no. 3, pp. 2448–2461, Mar. 2017.

[24] H. Wang, "Full-diversity uncoordinated cooperative transmission for asynchronous relay networks," *IEEE Trans. Veh. Technol.*, vol. 66, no. 1, pp. 468–480, Jan. 2017.

[25] K. J. Kim, H. Liu, M. Wen, P. V. Orlik, and H. V. Poor, "Secrecy performance analysis of distributed asynchronous cyclic delay diversity-based cooperative single carrier systems," *IEEE Trans. Commun.*, vol. 68, no. 5, pp. 2680–2694, May 2020.

[26] *A Precision Clock Synchronization Protocol for Networked Measurement and Control Systems*, Standard 1588-2008, Jul. 2008.

[27] A. Garg, A. Yadav, A. Sikora, and A. S. Sairam, "Wireless precision time protocol," *IEEE Commun. Lett.*, vol. 22, no. 4, pp. 812–815, Apr. 2018.

[28] K. J. Kim, H. Liu, H. Lei, Z. Ding, P. V. Orlik, and H. V. Poor, "A dCDD-based transmit diversity scheme for downlink pseudo-NOMA systems," *IEEE Trans. Wireless Commun.*, vol. 20, no. 2, pp. 1217–1232, Feb. 2021.

[29] L. Deneire, B. Gyselinckx, and M. Engels, "Training sequence versus cyclic prefix-a new look on single carrier communication," *IEEE Commun. Lett.*, vol. 5, no. 7, pp. 292–294, Jul. 2001.

[30] Y. Zeng and T. Sang Ng, "Pilot cyclic prefixed single carrier communication: Channel estimation and equalization," *IEEE Signal Process. Lett.*, vol. 12, no. 1, pp. 56–59, Jan. 2005.

[31] K. J. Kim and T. A. Tsiftsis, "Performance analysis of QRD-based cyclically prefixed single-carrier transmissions with opportunistic scheduling," *IEEE Trans. Veh. Technol.*, vol. 60, no. 1, pp. 328–333, Jan. 2011.

[32] G. Wu, Q. Du, and K. Hua, "Selective random CDD enhanced joint cooperative relay and HARQ for delay-tolerant vehicular communications," *Int. J. Distrib. Sensor Netw.*, vol. 11, no. 5, May 2015, Art. no. 657938.

[33] H.-S. Liao, P.-Y. Chen, and W.-T. Chen, "An efficient downlink radio resource allocation with carrier aggregation in LTE-advanced networks," *IEEE Trans. Mobile Comput.*, vol. 13, no. 10, pp. 2229–2239, Oct. 2014.

[34] C. G. Tsinos, F. Foukalas, and T. A. Tsiftsis, "Resource allocation for licensed/unlicensed carrier aggregation MIMO systems," *IEEE Trans. Commun.*, vol. 65, no. 9, pp. 3765–3779, Sep. 2017.

Authorized licensed use limited to: Princeton University. Downloaded on May 27,2022 at 01:57:22 UTC from IEEE Xplore. Restrictions apply.

[35] P. G. Moschopoulos, "The distribution of the sum of independent gamma random variables," *Ann. Inst. Stat. Math.*, vol. 37, no. 3, pp. 541–544, Dec. 1985.
[36] I. S. Gradshteyn and I. M. Ryzhik, *Table of Integrals, Series, and Products*. New York, NY, USA: Academic, 2007.
[37] A. P. Prudnikov, Y. A. Brychkov, and O. I. Marichev, *Integral Series*. vol. 3. London, U.K.: Gordon and Breach, 1992.
[38] *Further Enhancements to LTE Time Division Duplex (TDD) for Downlink-Uplink (DL-UL) Interference Management and Traffic Adaptation*, document TR 36.828 (V11.0.0), 3GPP, Jun. 2012.
[39] N. Balakrishnan, "Permanents, order statistics, outliers, and robustness," *Revista Matemática Complutense*, vol. 20, no. 1, p. 7107, Mar. 2007.

Kyeong Jin Kim (Senior Member, IEEE) received the M.S. degree from the Korea Advanced Institute of Science and Technology (KAIST) in 1991 and the M.S. and Ph.D. degrees in electrical and computer engineering from the University of California, Santa Barbara, CA, USA, in 2000.

From 1991 to 1995, he was a Research Engineer with the Video Research Center, Daewoo Electronics Company Ltd., South Korea. In 1997, he joined the Data Transmission and Networking Laboratory, University of California. After receiving his degrees, he joined the Nokia Research Center and Nokia Inc., Dallas, TX, USA, as a Senior Research Engineer, where he was an L1 Specialist, from 2005 to 2009. From 2010 to 2011, he was a Visiting Scholar with Inha University, South Korea. Since 2012, he has been a Senior Principal Research Staff with the Mitsubishi Electric Research Laboratories, Cambridge, MA, USA. His research interests include transceiver design, resource management, scheduling in the cooperative wireless communications systems, cooperative spectrum sharing systems, physical layer secrecy systems, device-to-device communications, local and private 5G networks, and AI-based smart grid systems.

Dr. Kim received the Best Paper Award in the 2014 IEEE-Chinacom, the IEEE ICC-2019, and the IEEE PES-GM 2020. He served as an Editor for IEEE COMMUNICATIONS LETTERS, a Guest Editor for the *IET Communications* Special Issue on Secure Physical Layer Communications, and a leading Guest Editor for the IEEE JOURNAL ON SELECTED AREAS IN COMMUNICATIONS Special Issue on Spatial Modulation for Emerging Wireless Systems. He currently serves as a leading Guest Editor for the IEEE JOURNAL OF SELECTED TOPICS IN SIGNAL PROCESSING Special Issue on Advanced Signal Processing for Local and Private 5G Networks and an Editor for the IEEE TRANSACTIONS ON COMMUNICATIONS.

Phee Lep Yeoh (Member, IEEE) received the B.E. (Hons.) and Ph.D. degrees from The University of Sydney (USYD), Australia, in 2004 and 2012, respectively. From 2012 to 2016, he was a Lecturer and a Research Fellow with the University of Melbourne, Australia. Since 2016, he has been a Senior Lecturer with the School of Electrical and Information Engineering, USYD. He was a recipient of the 2020 USYD Robinson Fellowship, the 2018 Alexander von Humboldt Research Fellowship for Experienced Researchers, and the 2014 Australian Research Council (ARC) Discovery Early Career Researcher Award (DECRA). He has received best paper awards from the IEEE ICC 2014 and the IEEE VTC Spring 2013, and best student paper awards with his supervised students from the 2013 and 2019 Australian Communications Theory Workshop (AusCTW).

Hongwu Liu (Senior Member, IEEE) received the Ph.D. degree from Southwest Jiaotong University in 2008. From 2008 to 2010, he was with Nanchang Hangkong University. From 2010 to 2011, he was a Post-Doctoral Fellow with the Shanghai Institute of Microsystem and Information Technology, Chinese Academy of Sciences. From 2011 to 2013, he was a Research Fellow with the UWB Wireless Communications Research Center, Inha University, South Korea. From 2017 to 2018, he was a Research Professor with the Department of Information and Communication Engineering, Inha University. Since 2014, he has been an Associate Professor with Shandong Jiaotong University. His research interests include MIMO signal processing, cognitive radios, cooperative communications, wireless secrecy communications, and future IoT.

Jianlin Guo (Senior Member, IEEE) received the Ph.D. degree in applied mathematics from the University of Windsor, Windsor, ON, Canada, in 1995. He is currently a Senior Principal Research Scientist with Mitsubishi Electric Research Laboratories, Cambridge, MA, USA. His research interests include coexistence of the heterogeneous wireless networks, time sensitive networking, edge computing for vehicular networks, networked control systems, fault detection in industrial automation, routing and resource management in wireless IoT networks, and nonlinear stability of convection in porous medium. He is currently an IEEE 802.19.3 Task Group Technical Editor.

Philip V. Orlik (Senior Member, IEEE) was born in New York, NY, USA, in 1972. He received the B.E., M.S., and Ph.D. degrees in electrical engineering from the State University of New York at Stony Brook, Stony Brook, NY, USA, in 1994, 1997, and 1999, respectively.

In 2000, he joined Mitsubishi Electric Research Laboratories Inc., Cambridge, MA, USA, where he is currently the Manager of the Electronics and Communications Group. His primary research interests include advanced wireless and wired communications, and sensor/IoT networks, and other research interests include vehicular/car-to-car communications, mobility modeling, performance analysis, and queuing theory.

Yukimasa Nagai (Senior Member, IEEE) received the B.E. and M.E. degrees in information and communication engineering from The University of Electro-Communications, Tokyo, Japan, in 1998 and 2000, respectively. He has been working with the Information Technology Research and Development Center, Mitsubishi Electric Corporation, Kamakura, Japan, from 2000 to 2016 and since 2020. From 2016 to 2020, he was with Mitsubishi Electric Research Laboratories, Cambridge, MA, USA. His research interests include wireless communication systems, signal processing, connected car, and the IoT. He has been involved in various standardization groups organized for Wi-Fi Alliance and IEEE 802.11/15/19. He served as a Vice Chair for Wi-Fi Alliance DSRC MTG from 2015 to 2018. He currently serves as a Vice Chair for Wi-Fi Alliance Automotive MSTG.

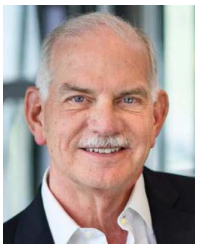

H. Vincent Poor (Life Fellow, IEEE) received the Ph.D. degree in electrical and computer engineering from Princeton University in 1977.

From 1977 to 1990, he was on the faculty of the University of Illinois at Urbana–Champaign. Since 1990, he has been on the faculty at Princeton, where he is currently the Michael Henry Strater University Professor. From 2006 to 2016, he served as the Dean of Princeton's School of Engineering and Applied Science. He has also held visiting appointments at several other universities, including most recently at Berkeley and Cambridge. His research interests include information theory, signal processing and machine learning, and their applications in wireless networks, energy systems, and related fields. Among his publications in these areas is the forthcoming book *Machine Learning and Wireless Communications*. (Cambridge University Press, 2021).

Dr. Poor is a member of the National Academy of Engineering and the National Academy of Sciences. He is also a Foreign Member of the Chinese Academy of Sciences, the Royal Society, and other national and international academies. Recent recognition of his work includes the 2017 IEEE Alexander Graham Bell Medal and a D.Eng. (honoris causa) from the University of Waterloo awarded in 2019.

Authorized licensed use limited to: Princeton University. Downloaded on May 27,2022 at 01:57:22 UTC from IEEE Xplore. Restrictions apply.